CHAPTER 5

Analysis and Evaluation of Aging Phenomena in PEMFCs

François Lapicque,* Caroline Bonnet, Bo Tao Huang, and **Yohann Chatillon**

Contents

1. Introduction 266
2. Degradation Phenomena in PEM Fuel Cells and Their Investigation Techniques 269
   2.1 Membranes 270
   2.2 Catalyst layers 273
   2.3 Gas diffusion layers 277
   2.4 Bipolar plates and other cell components 278
3. Experimental Aging Protocols 279
   3.1 Introduction and impact of the measurements made for aging evaluation 279
   3.2 Aging at constant current density: Single cells and stacks 281
   3.3 Periodic variations of voltage or current density 284
   3.4 Poor humidification of the reacting gases 289
   3.5 Freezing effect 292
   3.6 The case of contaminants 294
4. Literature Examples of Fuel Cell Aging 299
   4.1 Coupled membrane and catalytic layer degradation 300
   4.2 Effect of RH cycling, case of long periods 304
   4.3 Degradation of bimetallic alloy catalysts in PEMFCs 309
   4.4 Examples of FC contamination 314
   4.5 Aging by shutdown/start-up procedure 319

Laboratory for Reactions and Chemical Engineering, CNRS-Université de Lorraine, Nancy, France
* Corresponding author, E-mail address: francois.lapicque@ensic.inpl-nancy.fr

Advances in Chemical Engineering, Volume 41
ISSN 0065-2377, DOI: 10.1016/B978-0-12-386874-9.00009-9

5. Summary and Conclusions 324
References 327

Abstract Aging phenomena of fuel cells are of tremendous importance for scientists, developers, or users of fuel cells. Better understanding of aging phenomena in fuel cells—here polymer exchange fuel cells (PEMFCs)–is a necessary step in view to improving technology of the various components of PEMFC. In addition to a rapid description of recent progresses in the area, the chapter is aimed at giving a few ideas, a few concepts for investigation of aging phenomena, with sort of engineering, down-to-earth point of view. It was therefore preferred to emphasize here on methods for aging investigation and characterization, with a couple of representative examples in the area, as a complementary tool to more exhaustive, formerly published reviews on the various physicochemical phenomena.

1. INTRODUCTION

Polymer electrolyte membrane fuel cells (PEMFC) fuel cells have been the topics of numerous scientific and technological improvements for at least two decades. As presented more in details in the previous chapters, a fuel cell consists of a stack of individual, single cells connected electrically in series together with its environment for fuel preparation and management of the energy produced. Single cells likewise most electrochemical cells are formed from various components in a filter-press configuration. The electrolyte membrane usually being 15–25 μm thick separates two thin electrodes consisting of fine catalyst particles which are often deposited on a carbon black support: the three-layer sandwich constitutes the membrane electrode assembly (MEA). Besides, the gas fed by the so-called bipolar plates through millimetric ducts or patterns is more finely distributed through the gas diffusion layers (GDL) with pore size varying from 1 to 50 μm for the sake of uniform access of the reactants to the catalyst particles, being in most cases by Pt or Pt-based alloy nanosized clusters. The cell performance is governed by its components, but the technique employed for MEA preparation has a significant role too, in addition to the operation conditions as discussed later.

This energy conversion technology appears now as promising owing to its high efficiency, its convenient operation, and the reduced emissions to environment. PEM fuel cells are usually considered as reliable tools for energy production in both stationary and mobile applications. However,

the large-scale industrialization of this energy conversion technology is hindered by two main issues. First, investment costs of fuel cells are still far too high for possible competition with conventional technologies, such as internal-combustion engines. DOE target of fuel cell costs was actually of \$50/kW in 2010 and has been recently been announced at \$30/kW by 2015 (Wang *et al.*, 2011). The second hindrance is related to fuel cell durability and reliability as explained below. Durability is linked to lifetime: it can be defined as the aptitude to be operated with sufficient efficiency for a large period of time even though it is often dealt with as a time period. Reliability is the capacity of the considered object or process to be operated without risk of failure: in the present case, it is for the continuous, failure-free and hazardless production of energy.

For transported applications, hydrogen fuel cell power systems should be as reliable and durable as internal-combustion engines, that is, offering a 5000h operating lifetime, that is, approximately 7months under operating conditions, which can be prone to accelerated aging of the fuel cell by sudden loading changes, idle operation, unsuitable humidity, excessive temperature, presence of contaminants in the reacting gases, or freeze/thaw cycles. The lifetime expectancy of stationary fuel cell systems has to meet the target estimated by DOE at more than 40,000h. The durability of PEM fuel cell systems depends on the technology retained for both components and their assembly, and it has also been improving these past years. However, the current lifetimes of fuel cell vehicles and stationary power systems have been estimated at 1700 and 10,000h, respectively (Payne, 2009), far below the above targets. For the case of direct methanol fuel cells, the life expectancy is noticeably lower, making this technology less competitive, in spite of the advantages offered by the liquid fuel, being of far higher energy density than the light gaseous hydrogen. In this chapter, unless specified, the case of hydrogen PEM fuel cells will be treated.

The search of higher fuel cell durability may be hindered by the development of cheaper cell components involving largely reduced amounts of raw materials. For instance, the development of low-Pt charge electrode catalysts is also a crucial point in the competitiveness of fuel cells: electrode materials with Pt charge as low as $10\,\mu g\,cm^{-2}$ and offering comparable electrochemical performance as conventional catalysts have been found; however, in most cases, their performances were observed to decline dramatically within a few hundred hours. Likewise, MEA components developed two decades ago, with 175–250 μm membranes and Pt charges over $1\,mg\,cm^{-2}$, had been successfully used in long-term tests over several thousands of hours. Durability in spite of its significance cannot be investigated and improved regardless of the search of components whose manufacture can meet more easily the constraints of limited resources, in particular, of noble metal catalysts.

In spite of the considerable efforts in terms of investment and manpower during the past two decades, intensive R&D investigations have still to be carried for the design of fuel cells offering higher durability and reliability. For this purpose, mechanisms of aging occurring in fuel cells under nominal conditions or under accidental mode have to be better understood: the hurdles exhibited by a given fuel cell technology will then be identified before technological solutions can be imagined and tested for the improvement of the cell components.

- For the current hydrogen fuel cell technologies, the average decay of the single cell voltage at usual current densities—in the order of 0.5–1 A cm^{-2}—is in the range 2–10 $\mu V h^{-1}$, which corresponds to a reduction in the cell voltage for a 5000 h test from 10 to 50 mV. For methanol fuel cells (DMFC), the current density applied is usually lower, allowing cell voltage in the order of 0.5 V: the lifetime of such cells may be lower than those for hydrogen fuel cells. As expected, operation under less favorable conditions is to greatly increase the decay rate. It has to be mentioned at this point that the end of life of a cell under practical operation of energy conversion does not correspond to the utter collapse of the cell with negative values of the cathode-to-anode potential difference, but to a well-defined loss in the cell performance: 20% loss is frequently considered as corresponding to the end of life. For cells operated at constant current density, this means a 20% reduction in the cell voltage. As explained more in details in the following sections, the degradation of fuel cells performance is caused by degradation of the properties of one or several components: lower conductivity of the membrane, reduced catalyst efficiency, insufficient removal of liquid water from the GDL, and the bipolar plates by reduced hydrophobicity of these components. The degradation of the various cell components has been largely investigated and discussed depending on the operating conditions applied for the energy conversion, as reported in review papers (Borup *et al.*, 2007; Knights *et al.*, 2004; Schmittinger and Vahidi, 2008; Wang *et al.*, 2011; Zhang *et al.*, 2009a).
- Besides, durability and reliability of new fuel cell components or cells have to be determined in view to evaluate their potential larger-scale production: because of their long lifetime expected, it has appeared necessary to design protocols accelerated stress tests (AST), which are to provide an answer within experiment time far lower (often from 5 to 20 times lower) than the lifetime under nominal conditions: AST may consist in applying potential or humidity cycling, or excessive temperature, or operating in the presence of gas contaminants. Such accelerated test protocols have to be designed with care so that the information yielded can be extrapolated to real production conditions: if an AST

reveals that Cell A is better than Cell B, Cell A is expected to exhibit higher durability than Cell B in real operation. In addition, completion of AST with a given cell technology does not have to induce additional degradation phenomena which would not be observed under regular conditions. Finally, AST protocols may have to be modified for better fit to a novel cell technology.

The chapter was not designed to be one more review on the physical phenomena occurring in fuel cell degradation, and the readers are invited to refer to the above quoted papers. In particular, electrochemical processes in catalysts aging have been described by numerous authors, for example, Ferreira *et al*. (2005), Guilminot *et al*. (2007a,b), and Wu *et al*. (2008). Although the main phenomena are also briefly described here, the chapter was more targeted at the methods and the models that be used by engineers for better evaluation of aging processes in the investigated fuel cell system or to improve their design. Following this introduction, Section 2 briefly introduces the main degradation phenomena occurring in the various parts in the fuel cell, together with the available experimental techniques for evidence or quantitative evaluation of the degradation. The various operating conditions applied in long-term tests of AST protocols for observation of one fuel cell component are presented in Section 3: analysis of the operating variables is conducted in relation to the observed phenomena, with attempts in methodological approach. Section 4 presents a selection of significant examples of aging situations: in addition to summarized up-to-date conclusions reported in the literature, we present here a transverse discussion on physical phenomena, with integration of engineering reflection into the physicochemical description of facts. Covering the integrality of the various aging phenomena would be poorly realistic in the volume chapter and would be redundant with formerly published reviews documents in the area: it was therefore preferred to treat specific cases of practical significance from the engineering point of view.

2. DEGRADATION PHENOMENA IN PEM FUEL CELLS AND THEIR INVESTIGATION TECHNIQUES

The various components undergo their own degradation phenomena, and their durability differs noticeably from each another, as explained below. Sheets of polymeric membranes submitted to partly humidified hydrogen or oxygen exhibit little change in their swelling capacity by water uptake, even after more than 10,000 h provided the temperature of the cell is in the range recommended by the supplier. High durability of

single Pt/C electrodes has been observed for potentials below 0.8 V/RHE. Membrane electrode assemblies usually appear more sensitive to aging, and numerous investigations with MEA aging reported significantly reduced performance after from 2- to 10,000-h operation: compared behaviors of the MEA and of its single components indicate the lumped nature of membrane and catalyst degradation. The intrinsic durability of GDL, seals, and carbon-based bipolar plates is usually reported as good, that is, over 10,000 h. Finally, stack operation differs from single cell operation with respect to performance degradation and the lower durability usually reported for stack modules can be caused by the following facts:

- In most stack modules, cooling is achieved by water circulation in one dedicated plate over the other: the temperature of one cell usually differs by 1 or 2 °C from the neighboring cells. In addition, it is frequent that the two external cells at the stack extremities have temperature levels a couple of Celsius below that in the rest of the stack.
- In spite of the improvements made in the distribution of gas through the cells in the stack owing to progresses made in miniaturized reactors, slight local variations in the inlet gas flow rates can exist, resulting in local variations in pressure drop and efficiency, with possible variations in the deactivation rates of the catalyst.
- Mechanical constraints in the stack module: although care is taken in mounting the cells to buildup the stack, the likely unevenness in the Torque applied in the bolts, in addition to the temperature variations in the stack can be the cause of local privileged degradations of the GDL or the seals.

2.1 Membranes

Degradation of the membrane depends on the chemical nature of the electrolyte polymer (ionomer) employed: most relevant published investigations deal with perfluorosulfonic acid (PFSA)-based polymers such as Nafion® produced by DuPont or Gore Primea® by Gore: these polymers are good ionic electrical conductors provided sufficient hydration of their chains. Along time, polymer membranes can suffer from mechanical, chemical, and thermal degradation, depending on the operation conditions. Chemical degradation can occur under the action of hydrogen peroxide radical HO_2—together with OH—which can be produced through various chemical or electrochemical reactions in the cell. It can be noticed that the presence of metal cations generated by corrosion greatly catalyzes the radical formation. The above radicals formed attack the side sulfonate-containing chain of the polymer or its backbone, and the presence of Pt in the neighborhood is known to greatly catalyze the

degradation. In numerous investigations, fuel cell membranes are reported to undergo substantial thinning, which is to affect its mechanical resistance but without indication of its physical meaning. In most cases, membrane thinning is caused by both appreciable loss of the solid polymer to soluble smaller molecules and ions, for example, sulfonate and fluoride—and the likely reduction in the porosity of the polymeric structure, corresponding to lower water uptake. Mechanical degradation is due to the finite resistance of the polymer materials to repeated swelling and shrinking processes occurring under periodic variations of the relative humidity (RH) of the feed gases: this degradation leads to the formation of cracks, tears, punctures, or pinholes (Figure 1). Pressure difference between anode and cathode compartments is also to favor mechanical degradation. Finally, thermal degradation is caused by excessive temperature—and/or insufficient gas humidity: excessive dehydration of the polymer results in reduced electrical conductivity and can alter the mechanical property of the polymeric foil. In particular, PFSA membranes hardly tolerate temperatures over 100°C in long-term operations. Reinforcement of PFSA membranes by insertion of a harder-material mesh or by addition of PTFE or oxides particles allows better resistance of the composite materials obtained to degradation. Besides, alternative polymers such as polybenzimidazole, with possible impregnation of phosphoric acid, or PEEK-based polymers can allow higher temperature operations. In addition, because of their far lower water uptake in comparison to the conventional PFSA-based polymers, they are probably less sensitive to variations of the RH in the cell. However, relatively few results of aging tests of these polymers have been published up to now.

The extent of membrane degradation can be evaluated by using several techniques as follows (Table 1).

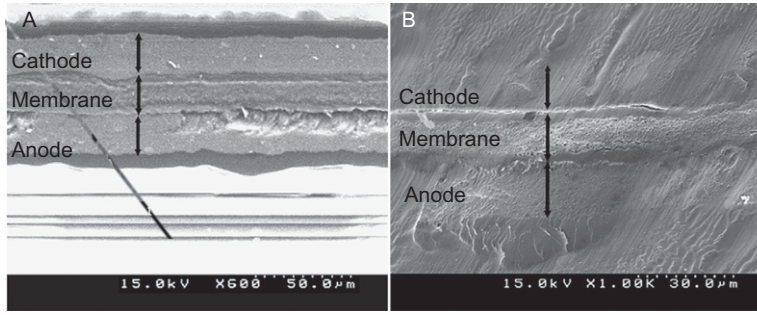

Figure 1 SEM view of MEA (Seo *et al.*, 2011): (a) Fresh MEA and (b) after on–off pulsation (5 and 10 min, respectively) with full humidification of fed air.

Table 1 Main techniques used for evaluation of membrane degradation

Technique	Variable measured	Reference
Water balance	Water amounts at the cell outlets	
EIS	High-frequency resistance	
Chemical analysis of water fractions	Amounts of F and S elements in water	
Chemical titration	Ion-exchange capacity	Inaba (2006)
NMR, MRI	Water content in the polymer	Bedet *et al*. (2008)
FT-IR	Presence of chemical species/ groups	
TGA	Membrane loss by thermal degradation	
Cyclic voltammetry with H_2/N_2	Hydrogen crossover	FCtestnet
Mechanical tests	Tensile strength, Young modulus	
Pressure measurements	Pressure transients in closed cells	

- Water balance consists in comparing the fluxes supplied by the humidifier upstream of the cell plus the flow rates of water produced by the electrochemical combination of oxygen with hydrogen, to the amounts of water contained in the two outlet gas streams. The water transfer coefficient α is usually introduced to express the significance of water flow rate transported from the cathode to the anode taking into account the amount of water produced as follows:

$$\alpha = \frac{N^{a}_{w,outlet} - N^{a}_{w,inlet}}{N_{w,prod}} \quad (1)$$

where subscript w refers to water and exponent a corresponds to the anode. Coefficient α indicates on the significance of electroosmosis transport rate (toward the cathode) in comparison to diffusion flux, most often from the cathode side to the anode. Change in the coefficient value along time reveals a change in water transport phenomena, corresponding, for instance, to a change in the overall diffusion of water through the membrane. In addition, an excess of water collected at the outlet streams in comparison to the ''inlet plus production'' flow rate reveals the side formation of water by electroless reactions between diffusing hydrogen

to the cathode chamber and the inlet oxygen—and the reverse in the anode chamber to a lower extent.

- The high-frequency resistance deduced from electrochemical impedance spectroscopy (EIS) is to correspond to the ohmic resistance of the cell: this resistance is often assimilated to the membrane resistance, assuming for this purpose negligible contribution from the electrodes, the GDL, and the bipolar plates. For aging cells, contact resistances due to partial delamination of the various layers may also appear and lead to overestimate the actual membrane resistance.
- Chemical analysis of the water fractions collected by ion chromatography leads to the loss in sulfonate and fluorine species from the polymer: the loss in fluorine is often considered as being an indicator of chemical decomposition of the polymeric membrane. In addition, compared amounts of F and S lost from the membrane may indicate on whether the cleavage induced by peroxide radicals concerns the polymer backbone or mainly its S-containing side chain, as proposed by Franck-Lacaze *et al.* (2010). Moreover, for the case of bi- or trimetallic catalysts, chemical analysis allows determination of the amounts of the metal cations accumulated in the MEA by the catalyst dissolution or by corrosion of the end plates and which cannot be reduced back by hydrogen like Pt—Pt recrystallization presented in Section 4.1.
- *Ex situ* determination of the ion-exchange capacity of the polymer can be examined in relation to the loss in sulfonate group and the change in ohmic resistance.
- Magnetic resonance imaging techniques can be used successfully for determination of the local water content in the membrane bulk. However, the signal emitted with thin membranes may be too low for accurate measurement and global NMR measurements with accumulation of the signal are then preferred.
- Determination of the fuel crossover by linear sweep voltammetry at low scan rates—$2\,mV\,s^{-1}$ for instance—may be affected by the RH of the gases fed to the cell: the accuracy of the technique has to be controlled, in particular, for significant crossover flow rates. For significant leaks in the membrane foil, pressure tests represent a complementary experimental technique for evaluation of the mechanical degradation.
- Finally, measurement of the mechanical properties can be done only *ex situ* with the bare polymeric membrane.

2.2 Catalyst layers

Catalyst layers (CL)—or electrodes—can suffer from the loss in catalyst activity to change in morphology of the catalyst clusters. For instance, Pt catalysts can be subject to dissolution at high cathode potential—that is, at

low or nil current density—or in the presence of oxidant compounds, for example, radicals, leading to the various phenomena depicted in Figure 2. First, the dissolution can be followed by transport of the ions in the water-rich gel and back reduction process at the surface of another Pt cluster: the overall phenomenon often referred as the Oswald ripening phenomenon (Figure 2a) leads to growth of the larger catalyst particles. Besides, Pt cations diffusing in the ionomer bulk can reduce to metal Pt by action of crossover hydrogen after a chemical process, resulting in the formation of Pt particles in the membrane bulk (Figure 2b). Finally, Pt particles can migrate on the surface of the carbon support and coalescence to form larger particles (Figure 2c). The case of Pt-based bimetallic catalysts is more complex depending on the nature of the other metals and is discussed in Section 4.3.

The carbon support of the electrode is prone to corrosion, in particular, under the catalytic action of platinum: appreciable corrosion can actually be observed above 0.55 V/RHE (Roen *et al.*, 2004). Corrosion of the carbon particles is expected to result in CO_2 formation. Moreover, even though carbon particles are seldom entirely dissolved, partly corroded particles are prone to detach from the electrode structure, together with the attached catalyst clusters: this results in additional loss in electrode activity. Besides, apart from corrosion, the significant reduction in the electrode thickness evidenced by SEM observations after long-term operations can be largely due to compaction of the carbon structure

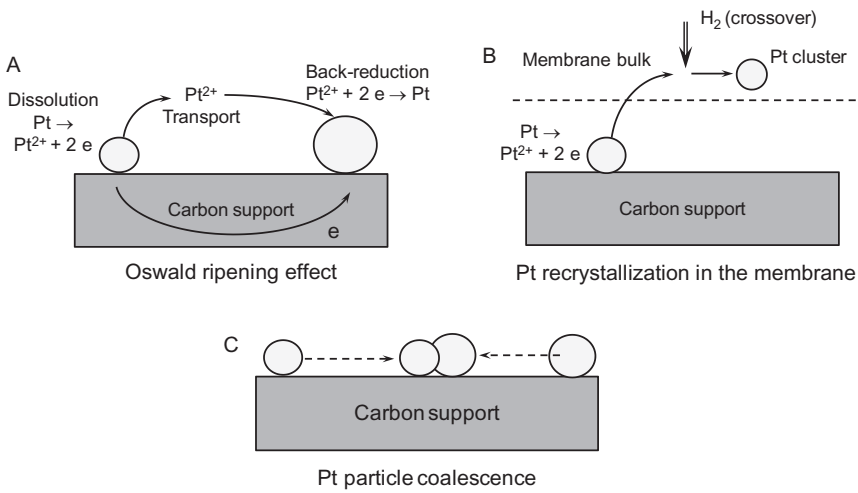

Figure 2 Platinum dissolution and recrystallization in a PEMFC: (a) Ostwald ripening effect, (b) platinum precipitation in the ionomer, and (c) coalescence of Pt particles.

whose initial porosity can attain 80% for a fresh MEA. The increased compactness is usually far more significant near the edge of the bipolar plate pattern than near the channel.

Finally, the thin ionomer layer in contact with the catalyst cluster and facilitating proton transfer to or from the electrode surface can also be degraded along time: this will be discussed more in details in Section 4.

The current investigation techniques of degradation of the CLs are reported in Table 2.

- The most conventional feature of a fuel cell system is probably its voltage versus current density curve, also often referred to polarization of performance curve. In spite of its importance in the assessment of its performance, the experimental procedure for its acquisition is seldom described in details. As a matter of fact, in numerous papers, no indications on the electrical mode are given: was the cell voltage monitored at fixed current density until steady state was observed, or was the current scanned at a nonspecified rate? Depending on the technique used, differences in the cell voltage up to 80 mV at middle-range current density can be observed. Moreover, in some published reports, it is not expressed whether the data were observed at fixed flow rate of the reacting rates or at fixed stoichiometric coefficient.

Table 2 Main techniques used for evaluation of catalyst layer degradation

Technique	Variable measured or observed	Reference
Cyclic voltammetry	Electrode activity: $I-E$ variations	
	Electrode active surface (EAS)	Pozio *et al.* (2002)
EIS	Charge transfer resistance	
	Electrode capacitance	
Chemical analysis	Pt content in the MEA	
SEM	Overall morphology, layer adherence	
TEM	Catalyst morphology, particle size	
XRD	Catalyst structure, particle size distributions	
EPMA	Element analysis: evidence of impurities	
XRF	Element analysis: evidence of impurities	
XPS	Evidence of oxidized surface groups	Avasarala *et al.* (2011)

- Apart from the polarization curve, the electrode activity can be qualitatively evaluated by cyclic voltammetry or by EIS at various current densities: EI spectra usually consist of two main loops: the feature obtained at high- or middle-range frequencies corresponds to charge transfer phenomena and the other at frequencies below 1 Hz being for diffusion control. Because oxygen reduction is a far slower process than hydrogen oxidation, the loop related to hydrogen oxidation—although at higher frequency—may be hardly distinguishable from the far large feature related to the cathode reaction. In most cases, comparison of the spectra recorded at regular intervals along the long-term run indicates on the cathode catalyst degradation: this is observed by increasing values for the charge transfer resistance and, in some cases, by changes in the capacitance of the cathode.
- Moreover, the electrode active surface (EAS) of the two electrodes can be determined by cyclic voltammetry from the adsorption–desorption curves assuming that the charge consumed for the oxidation of a hydrogen monolayer is $210\,\mu C\,cm^{-2}$ for polycrystalline Pt. The values for the EAS data obtained by this technique can be affected by the applied scan rate: $10–50\,mV\,s^{-1}$ is the usually recommended range. CO stripping is a derived electrochemical technique relying on the huge affinity of CO toward Pt surfaces. As a matter of fact, because different reaction mechanisms are involved in the two techniques, they lead to different, complementary information, as follows: (i) because H_2 oxidizes to H^+, use of hydrogen yields the surface of the catalytic sites in contact with the ionomer, with no indication of the amount of catalytic sites in contact with the reacting gas; (ii) CO oxidation is only possible where the catalyst is in electrical contact with the support, regardless of the local presence of the ionomer.
- The other techniques mentioned in Table 2 are for postmortem investigations. Chemical analysis of the MEA after total dissolution in strongly acidic solutions can lead to the amount of the platinum still attached to the catalytic layers, but the data obtained account for combined cathode and anode. It has nevertheless to be reminded that only the Pt surface of the triple contact area, that is, covered by the ionomeric thin layer and in contact with C is electrochemical active in polymer exchange fuel cell (PEMFC); therefore, the results of chemical analysis are not directly related to the electrode activity. SEM cross-sectional observations allow changes in the MEA morphology and in the cohesion of the various layers, to be followed by comparison with similar cuts with a fresh MEA. Qualitative analysis of the observations has to be performed with care since preparation of cross-sectional samples can be the source of local delamination which is not due to FC operations.

- For access to particle size, the simplest method relying upon Scherrer's formula might be of limited accuracy for polydisperse nanoparticles and can provide only an estimate for the average particle size. More sophisticated techniques are often preferred. Precise observations of the catalyst and of its support are possible with TEM, and particle size distribution can be drawn by computer treatment of the images produced. XRD can yield the structure of the catalysts: this is of moderate interest since commercial Pt catalysts usually do not have a unique crystalline structure. However, in most studies, Pt (220) peak is often considered in the treatment of XRD patterns to minimize the perturbation induced by the signals of the carbon support. Particle size distribution of the catalyst clusters can be yielded from analysis of XRD patterns using appropriate models since the measurements are made by averaging over the volume of the metal particles surrounded or not by the ionomeric layer, which limits the accuracy of the technique. Moreover, when used for MEA investigation, XRD technique characterizes the overall MEA including catalyst particles and agglomerates not only in the electrodes but also in the membrane bulk—this can be encountered after aging, as described in Section 3. For the above reasons, consistence between size distributions obtained by TEM and RXD may differ: care must be taken in the comparison of the two data sources. It is often considered that TEM yields more accurate results and that XRD is used for confirmation of the orders of magnitude. Finally, it can be noticed that, provided that the catalyst surface is 100% active, EAS and the particle size distribution should be in theory linked to each other.

2.3 Gas diffusion layers

Conventional GDLs are 150–400-μm thick sheets of fibrous conducting materials. GDL can be carbon papers, as Toray® paper, or cloth, exhibiting quite a softer mechanical structure. Carbon-based fibers are compacted to produce a felt-like structure with an average pore size ranging from 10 to 50 μm. The resulting porosity is usually in the order of 60–80%. Addition of 20–40% PTFE to the carbon-based material for the GDL manufacture brings its water-repellent property: liquid water formed at high current density or upon high hydration of the reacting gases can be efficiently removed from the fuel cell, then avoiding all flooding phenomena in the cell structure. Degradation of the GDL can be caused by two phenomena: (i) reduction in the average porosity of the GDL by the mechanical pressure applied to the cell components even under regular operations: this is particularly significant at the edge of the plate pattern, in comparison to the channel neighborhood; (ii) besides, the surface hydrophobicity

through decomposition of PTFE can be reduced by long-term operation or under oxidizing conditions, for example, for high cathode potentials or upon exposure to oxidizing gases. This change in surface properties can be evidenced as done, for instance, by Chen *et al*. (2009) with chemically aged GDLs.

In most recent FC technologies, the gas diffusion layers (GDL) actually consists of two layers: the mesoporous fibrous layer described above is covered by a microporous layer (MPL) made of carbon black particles and PTFE for sufficient hydrophobicity. This structure of finer porosity pressed against the CL allows more efficient transfer of the reacting gases toward the catalyst cluster. Aging of the cell is also to reduce progressively the porosity of the MPL and damage the water-repellent PTFE. The carbon materials used in the two GDL undergo little significant corrosion due to the absence of Pt which is to catalyze the electrochemical carbon oxidation; however, the carbon surface could be oxidized to phenols or quinone groups, even without too significant electrochemical dissolution.

Investigations conducted on the GDL of cells after end of life can be difficult, in particular, because electrode layers often strongly adhere to part of the GDL surface: the recovery of separate cell components is often troublesome and cannot be achieved after long-term operation. Measurements of the electrical conductivity of the obtained GDL, in comparison with a fresh GDL, are to give an overall response, accounting for the increase in compactness (corresponding to increased overall conductivity) and the possible formation of contact resistances due to the surface oxidation of the GDL chemical compounds.

2.4 Bipolar plates and other cell components

In conventional fuel cell technologies, bipolar plates are machined out of graphite, carbon-based composites, or polymer-based composites: the material employed has to ensure sufficient mechanical stiffness for possible connection of the cells into a stack and to exhibit good electrical conductivity. In addition, as for GDLs, their surface has to be sufficiently water repellent for efficient removal of the liquid water formed. Degradation of carbon- or polymer-based plates mainly concerns the change in surface state induced by the degradation of the water-repellent additive and also to a minor extent the surface oxidation of the carbon materials: evacuation of water from the channel is to be hindered, and contact resistance with the GDL may appear, affecting the overall conductivity of the cell or the stack.

Development of metal bipolar plates has been the topic of numerous investigations, in particular, because of the expected reduction in manufacture cost and weight offered by such technology. The metal materials

have to be perfectly corrosion resistant since most transition metal cations are powerful catalysts of the oxidations of both ionomer and catalyst supports, while poisoning the electrode catalyst. Apart from bulk corrosion, growth of superficial oxide layer, as chromium oxide at the surface of most stainless alloys, is the source of increased contact resistance. Suitable surface treatment by treatment ion sputtering or other dry techniques is to reduce the significance of this side phenomenon. XPS can be used as a postmortem technique for evaluation of the oxide layer formation, in addition with the measurement of contact resistances (Wang *et al.*, 2008b).

The available literature dealing with technological issues with seals or endplates or bus plates is actually very scarce. Polymeric seals used in most PEMFC are, however, prone to aging because of the relatively high temperature together with the pressure applied, and it is likely that the seals used in most current fuel cells could not prevent from gas leakages for year-long continuous operation: improvements in this component are also necessary for safe operation. The material used for endplates is of great importance since corrosion of copper-based alloys has actually been observed, together with the redeposition of the other metal on the other side of the plate and at the bipolar platen surface: the battery formed is to be the source of metal cations not so far from the MEA, which could poison the catalyst, be detrimental to the ionomeric membrane and modify the electrochemical behavior of the fuel cell.

3. EXPERIMENTAL AGING PROTOCOLS

In situ tests, that is, tests conducted with fuel cells under real operation provide information that can more easily be used in the evaluation or the development of fuel cell technologies. *Ex situ* tests are often of an easier achievement since they are carried out with only one cell component and in a bench-scale system. However, extrapolation of the data obtained after interpretation to the real electrochemical behavior of the cell investigated can be more difficult or of a restricted accuracy. This section deals with the various ASTs employed or developed depending on the nature of aging targeted, with emphasis on the methodology used for this purpose.

3.1 Introduction and impact of the measurements made for aging evaluation

Various protocols for investigation of fuel cell degradation can be considered. The most single protocol for this purpose is certainly the operation at constant performance, under the conditions recommended for reliable

operation of the fuel cell system. Other protocols inducing stronger stresses on one or several component of the cell are also described here, together with the procedures developed by DOE or USFC and considered as standardized protocols for possible comparison of various fuel cell technologies.

In all protocols for long-term fuel cell operations, various measurements are performed at regular intervals for evaluation of the degradation progress, as shown in Tables 1 and 2. Some of them such as chemical analysis of the water fractions collected do not affect the course of operation. Other measurement techniques, in particular, most electrochemical measurements by impedance spectroscopy or cyclic voltammetry, can affect the state of the fuel cell system. The impact of the electrochemical determination can be reversible or ''more irreversible,'' as explained below.

Short interruptions in long-term tests required to start impedance measurements induce a transient change in the electrode surface, and then the average cell voltage during the frequency scan may be somewhat higher than its level before the interruption: in most cases, the transient phenomenon occurs for a restricted period of time, that is, less than 1 h and is therefore reversible. Periods at open circuit voltage (OCV) longer than a few minutes are to change more durably the electrode state, enhancing, for instance, the surface oxidation of the platinum clusters and modifying the water management of the cell if the gases are continuously fed to the cell. Determination of the performance curve at steady state, with the measurement of the cell voltage for a number of current density levels, is to have a longer-term effect on the cell voltage, depending on the procedure chosen for the determination: continuous current scanning at appreciable scan rate, although less accurate, that is, less representative of real steady operation, is to affect less the operation state of the fuel cell than repeated steady measurements at fixed current density through an hour-long procedure.

Besides, cyclic voltammetry at low scan rate and for potentials lower than 0.5 V is known to allow reduction of the superficial oxide layer of the platinum clusters, resulting in larger performance of the cell after the determination. Although to a lower extent, voltammetry carried out at higher scan rates for estimation of the EAS can have similar effect: in both cases, the induced change in the fuel cell state appears reversible and corresponds to sort of catalyst regeneration. Figure 3 gives an example of cell voltage variation along time either for the case of a single cell at a current density corresponding to regular operation: the cell voltage after the electrochemical evaluation of the FC degradation is nearly 20–40 mV higher than before. Between two series of electrochemical characterization, the cell voltage decreases regularly with a rate in the order of 20–50 $\mu V h^{-1}$, before the following peak of cell voltage. However, the decay rate averaged over the whole sawtooth voltage profile is far

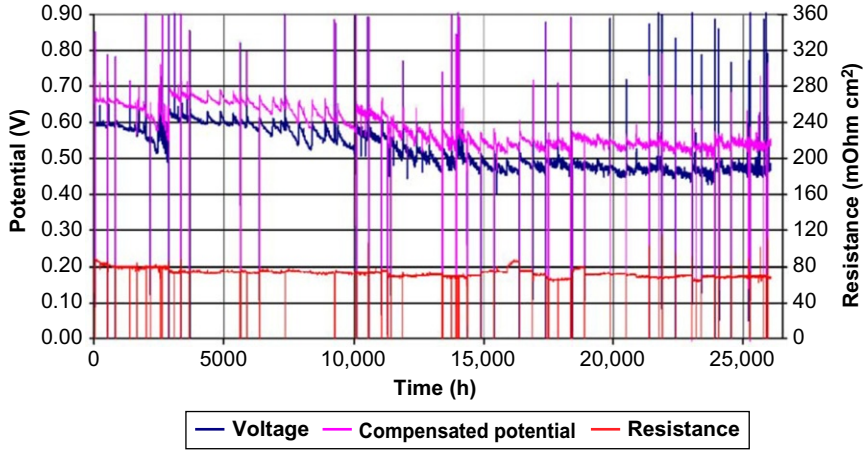

Figure 3 Examples of sawtooth voltage profiles in long-term runs of a single cell (Cleghorn *et al*., 2006).

lower, in the order of $4\mu V h^{-1}$ for the two cells: the regeneration allowed by the repeated cyclic voltammetric measurements, although not perfectly irreversible, appears to contribute to extend the cell lifetime. Moreover, Uribe and Zawodzinski (2002) reported regeneration of the cathode catalyst upon short period as 0.5V, after fuel cell aging as 0.8V.

Apart from the above procedures which have a positive effect on the fuel cell state, the various tests performed on a fuel cell and presented here can induce damage, degradation, and aging of the components. Some of the changes made are reversible as those induced by water management or short-term operation at high cathode potential inducing oxidation of the Pt surface for instance; others caused, for instance, by severe chemical contamination or more extreme steady or cycling conditions are irreversible, as for the case of Pt and carbon support dissolution or the membrane perforation.

3.2 Aging at constant current density: Single cells and stacks

3.2.1 Operations at nominal, regular current density

This type of aging procedure is currently seldom considered for single PEM hydrogen fuel cell investigation, except for comparison purpose with tests conducted under more extreme conditions as, for example, to test the tolerance of contaminants or dry operation exhibited by a new cell technology. In contrast, such tests are still currently made for assessment of stack durability.

Contrary to the case of hydrogen single cells, whose durability can exceed 10,000h, most investigations conducted with stacks have been

carried out for periods in the order of 2000 h. Longer runs have nevertheless been reported in the early 2000s by Ballard company, (Washington, 2000; Ahn *et al.*, 2002) who could run a short stack during 8000 h. Formerly, General Electrics (in 1979) had reported a 60,000 h test with a Nafion-based stack module operated with pressurized hydrogen/oxygen (LaConti *et al.*, 2003). However, little information on the state of the membrane or the catalysts along the long-term operation is given, and only the results of postmortem investigations have been reported. As explained by Cleghorn *et al.* (2006), the paucity of technical data is mainly the fact that much of this activity has been confined in the industrial sector. Nevertheless, St. Pierre and Jia (2002) reported on their successful test over 11,000 h with an average decay rate below $2\,\mu V\,h^{-1}$, with regular monitoring of kinetic, ohmic, and transport losses in the stack. Fuji Electrics could run a stack module over 15,000 h with no appreciable voltage loss at $0.4\,A\,cm^{-2}$ (Takahashi *et al.*, 2002). The longest continuous operation of a PEMFC stack described in the available literature was certainly achieved by Gore Inc. (Cleghorn *et al.*, 2006): the cell voltage variation in the 26,000 h run was near 110 mV at $0.8\,A\,cm^{-2}$, corresponding to an overall decay rate near $4\,\mu V\,h^{-1}$, even though far larger decay rate was recorded in the 500-h-long period between two electrochemical characterization of the cell state, as shown above in Section 3.1 and by Figure 3.

3.2.1.1 Case of DMFC cells Aging of single DMFC cells is still investigated prior to the observation of the electrochemical behavior of a stack. For such cells, as also for other alcohol fuels, research efforts have still been put for the search of catalysts exhibiting higher tolerance to CO than pure Pt and polymers having a lower fuel crossover than usual PFSA-based polymers. Catalysts—supported on carbon materials—are often binary metal catalysts, for example, Pt–Ru, or ternary systems such as Pt–Ru–Mo, whose stability at the anode has to be controlled. Contrary to hydrogen, oxidation of alcohols is a slow electrochemical process for which overpotentials can exceed 300 mV. Taking into account the equilibrium potential for methanol or ethanol oxidation, care has to be taken to maintain the anode potential below 0.5 V to avoid significant dissolution of Ru. Besides, hydrocarbon-based polymers can be preferred over PFSA-based polymers in the membrane, because of the far lower methanol crossover exhibited. However, the contact between the membrane and the carbon electrodes impregnated with Nafion is lower than that offered in Nafion-based MEA (Prabhuram *et al.*, 2010) and is more sensitive to aging, even at regular conditions for energy production. The current density range for ''regular'' aging is from 0.15 to $0.3\,A\,cm^{-2}$, corresponding to cell voltage in the order of 0.5 V.

Tests with DMFC stacks have been reported in the literature, most often with laboratory stacks as, for instance, by Jeon *et al*. (2007) or Dixon *et al*. (2011): the current density is usually below $0.2\,A\,cm^{-2}$ in tests conducted from 400 to 5000 h.

NB. In DMFC real systems, contrary to the case of single cells installed in a rig, the water produced at the anode is recycled and the operation reactants—humidified air and methanol solutions—may be contaminated by impurities accumulated in the stack along the run: this represents an additional cause of aging and an additional hindrance to the development of DMFC technology. The above issue may also be encountered in PEMFC systems with upstream hydrogen production module by hydrocarbon reforming: water management and reuse in the overall system, from the reforming chamber to the stack module, is possible, provided technological solutions relying for instance, upon ion exchange, be integrated in the system to avoid contamination of water and accelerated aging.

The data briefly reported here cannot be extrapolated directly to any type of stack modules, for a number of reasons. Because of the confidential character of such investigations, a couple of technical pieces of information, for example, flow pattern of the bipolar plates, seals, and GDL technology, have not been indicated in some of above papers. In most cases, robust components, for example, relatively thick membranes and large Pt loading in the CLs, had been selected. In addition, most tests presented above have been conducted under favorable operating conditions, for example, middle-range current density corresponding to cell voltage near 0.6 V or slightly more, fully humidified hydrogen and oxygen. As discussed in the following sections, modification of the operating conditions is to largely reduce the life expectancy of the stack to be tested. Finally, for practical production of energy in transported or stationary systems, the appreciable regeneration of the catalysts during the repeated electrochemical characterization phases cannot be expected, which is to significantly diminish the lifetime of the FC to be used, in comparison to that for laboratory investigations.

3.2.2 Operations at low current density

For systems producing electricity such as batteries or fuel cells, low current densities correspond to relatively high cell voltage, that is, in the order of 0.8 V. Such operations of energy systems may correspond to idle operations: for the example of stationary fuel cell systems, this operation mode is to be applied in periods of low energy demand. However, it can be regretted that the value of the low current density chosen in most papers is usually not justified as being representative of given practical operation the fuel cell systems. Operation at low current density often

appears implicitly as representing an AST and can be conducted also for fundamental purpose for better understanding of aging phenomena.

In hydrogen PEMFC, the anode overvoltage is often very low in comparison to that at the cathode, whose potential is therefore fairly close to the cell voltage. Operating at low current density generates oxidative conditions at the cathode, in particular, for the catalyst and its carbon support as briefly expressed in Section 2. Metal catalysts may dissolve to cations depending on standard potentials of the couple metal/metal cations. The case of some bimetallic catalysts is treated in Section 4. In addition, more severe degradation of the membrane polymer is observed, in particular, for PFSA-based polymers. The situation of DMFC is somewhat different because the overpotentials of the two electrodes have comparable absolute values, that is, attained rapidly 0.2 V even at very low current densities. This renders the degradation due to corrosion far less acute. Various papers deal with degradation phenomena for current density near 0.1 A cm^{-2} for hydrogen PEM cells and below with alcohol fuels: faster aging has been reported, for both the catalyst and the membrane, with decrease rate of the cell voltage far larger than 10 μV h^{-1}. Recently, Wu *et al.* (2010) could operate a six-cell PEM stack at 10 mA cm^{-2}: the cell voltage varied from 0.90 to 0.75 V along the 1200-h run. The high durability of the stack operated under such conditions was greatly due to the periodic transient regeneration of the cell allowed by the electrochemical characterization of the cell by cyclic voltammetry performed every 100 h.

Ex situ tests can also be conducted in liquid phase: the CL is fixed at a support electrode—often a rotating disk electrode—and the potential is submitted to variations from 0 to 1.2–1.5 V or above with moderate sweeping rates (Borup *et al.*, 2007; Roen *et al.*, 2004). Long-term tests (192 h) have also been carried out at 1.2 V by Shao *et al.* (2006).

3.3 Periodic variations of voltage or current density

3.3.1 Fluctuation periods and transients in fuel cells

Fuel cells can be operated with fluctuations of current density, resulting in time variations of the cell voltage, because of the time variations of the energy demand, in spite of the possible presence of batteries in cars, or connection to the grid for stationary applications: this arrangement allows responses of the overall energy production system faster than that allowed by the stack module surrounded with the fuel preparation and electricity management. The energy demand of stationary fuel cell systems is to vary along the day: the timescale of the demand fluctuations is in the order of the hour or more. For transported—mobile, automotive—applications, profiles of the energy demand exhibit different time constants,

with very short periods corresponding to acceleration or sharp reduction in the vehicle velocity, and longer periods with smoother fluctuations, as for driving outside urban areas. The period for the current or power cycling in emulation experiments has to be selected taking into account the targeted application.

Another constraint to be taken into account in the selection of the cycling frequency is the transient of the fuel cell response, which is governed by various physical phenomena. As revealed by impedance spectroscopy or other transient techniques, the electrochemical response of a fuel cell to a sudden change in power demand consists of several contributions:

- Ohmic drop linked to the finite conductivity of the cell components exhibits transients in the order of the millisecond or below.
- Transient charge transfer phenomena linked to charge/discharge of the electrode surface are visible within less than 1 s in most cases.
- Mass transfer phenomena, due to gas diffusion and/or water transfer: changing the cell voltage or the current density is to change the flux of water produced at the cathode, resulting in modified hydration in the membranes and electrodes. Transient diffusion in one-dimensional system (coordinate x) can be approached by Fick's second law:

$$\frac{\partial C}{\partial t} = D\frac{\partial^2 C}{\partial x^2} \tag{2}$$

where C denotes the local concentration and D is the diffusion coefficient. Solution of the above equation subject to the suitable boundary conditions let appear characteristic time, τ_m, equal to:

$$\tau_m = \frac{L^2}{D} \tag{3}$$

where L is the characteristic dimension. For the case of liquid water transport through the membrane, L may be taken as the membrane thickness. Consider a 20-μm-thick membrane and D in the order of $10^{-10}\mathrm{m^2s^{-1}}$ leads to τ_m=4 s: for such case, water management in the membrane can attain steady state within less than 1 min. The case of gas diffusion to the catalyst surface is more complex, because of the complex structure of the electrode, in the vicinity of the ionomeric layer and the catalyst cluster. However, impedance spectra of fuel cells under operation with low excess of air to the cathode often exhibit a loop—in the Nyquist plot—for frequencies ranging from 1 Hz down to 10 mHz: corresponding characteristic time ranges from 1 to 100 s. It can therefore be estimated that mass transfer phenomena in the cell can reach steady conditions within a few minutes.

- The time variations of the current density induce corresponding changes in the heat flux produced by the cell, which is to result in transient variations of the temperature in the MEA, the GDL, and the bipolar plates. Although the electrode kinetics depends on the local temperature, the main expected effect could be variations of the saturation pressure of the water pressure, depending on the cell configuration: single cells or stacks, temperature control of the cell by the presence of resistors or on the contrary by coolant circulation in the bipolar plates, etc. However, lower current density results in both lower heat and water production: therefore in such cases, the risk of water condensation in the GDL structure or the bipolar plates is reduced by the lower amount of water formed by the cathode reaction. In all cases, transient variations of temperature T can be modeled as done for concentrations: for the case of a one-dimensional system, the heat diffusion can be expressed by the partial differential equation:

$$\frac{\partial T}{\partial t} = \alpha \frac{\partial^2 T}{\partial x^2} \tag{4}$$

where α is the thermal diffusivity of the fluid or the medium considered. From the above equation, the characteristic time involved in the time variations of the temperature appears to be L^2/α. Heat transfer by diffusion can be caused by gases, liquid water (if any), and the solid media. Because of the high heat conductivity of the solids in presence, heat transfer in the solid can be considered as fast in comparison to that in the fluids (the membrane being a gel behaves more like a liquid than a pure solid). Thermal diffusivity of liquids largely exceeds mass diffusivity D, making the characteristic time τ_H far lower than τ_m. Transients of heat phenomena are then expected to occur in shorter periods of time than those for mass transfer. However, the change in the water management caused by the change in both heat and water flux produced is to induce transient diffusion of liquid water, the intensity, and the direction of which being dependent on the cell configuration and the operating conditions: the resulting transient behavior of the cell can therefore be considered to occur within comparable time lapses as those for mass transfer phenomena.

For the reasons given above, pulsations of relatively high frequency (over 0.01 Hz) are to impact mainly on the electrochemical state of the electrode, with nearly steady-state heat and water management in the cell. Conversely, fluctuations of current or potentials with periods larger than a couple of minutes will allow periodic changes in heat and water management.

3.3.2 Examples with periodic variations of current or voltage

Time variations of one electrical variable (E or i) other from pulsed variations can also be used: driving cycles established from emulation of transported applications allow the behavior of the fuel cells under real embarked conditions to be predicted: the accuracy of the procedure relying upon ASTs may depend on the relevancy of the cycle and probably to some extent to the cell itself. Besides, cyclic voltammetry can be used in more fundamental investigations, in particular, for investigation of the degradation of the CLs. Table 3 gives examples of published investigations. It has to be mentioned that even though a number of specific variation profiles of the electric variable have been imagined, tested, and reported in the literature, standard protocols for cell degradation have been developed, in particular, by the DOE and USFC in the USA (Garland *et al.*, 2007). Operations with H_2/air (or pure oxygen) correspond to real fuel cell operations, with cathode potentials below the OCV, in the order of 0.95–1V. The cathode behavior over this value can be observed by replacing the oxygenated stream by a feed of inert gas, for example, nitrogen or helium, which allows to follow, in particular, the electrochemical corrosion of the carbon support to carbon dioxide at potentials up to 1.5V. It may be expected that the results obtained for carbon corrosion under neutral gas at 1.5V cannot directly yield the corrosion rate of the support in the cell fed with H_2/air at OCV.

As shown in Table 3, most investigations made with periodic electrical variations could allow better understanding on catalyst degradation.

The time constant of the variations was in the order of 1min or less—except for the last example given; the flow rates of gas were maintained constant: for the reason given above, hydration of the membrane bulk cannot perfectly follow the fast variations and the change in hydration could be visible principally in the ionomeric layer in the electrodes. The electrode surface can undergo the fast variations of the electric variable, with probably transient oxidation of the platinum surface at high cathode potential, even within short periods, as explained below. As a matter of fact, Uribe *et al*. observed as expected the degradation of the Pt surface during the 600s at 0.8V; more surprisingly, the catalyst surface was shown to be regenerated within the 6-s-long step at 0.2V, indicating the short response time of the electrode surface to potential fluctuation.

The longer-period tests reported by Frank Lacaze *et al*. were carried at fixed stoichiometry at least for air introduction, avoiding drying of the cell in periods with low current densities. For this case, the cell could attain a steady behavior, with respect to electrochemical state as well as to heat and water management: such operation can be considered as the superimposition of long-term operations, and the results obtained are therefore comparable to long-term tests at low current density.

Table 3 Examples of aging investigations upon periodic variations of potentials or current density

Electrical variations	Time variable	Gas fed	FC components observed	Reference
Driving cycle		H_2/N_2	Carbon support	Borup *et al.* (2006)
Driving cycle		H_2/air	Catalyst, Nafion layer on the CL	Li *et al.* (2010)
CV: 0.04–1.2 V	$2\,mV\,s^{-1}$	H_2–N_2/He	Catalyst	Roen *et al.* (2004)
CV: 0.1–1.2 V	$10\,mV\,s^{-1}$	H_2/N_2	Catalyst	More (2005)
CV: 0.8–1.5 V	$100\,s^{-1}$	H_2/N_2	Catalyst	Borup *et al.* (2006)
0.2–0.8 V	6–600 s	H_2/air	Electrode; overall cell	Uribe *et al.* (2002)
0.6–OCV	150–30 s	H_2/air	Electrode: ESA	Jao *et al.* (2010)
0–$0.7\,A\,cm^{-2}$	10–5 min	H_2/air	Catalyst, membrane	Seo *et al.* (2011)
0.6–0.96 V		H_2/air	Catalyst	USFC
0.6–1.2 V		H_2/N_2	Catalyst	USFC
0.7–0.9 V	30–30 s	H_2/N_2	Catalyst	Garland *et al.* (2007)
0.02–$0.54\,A\,cm^{-2}$	>1–>1 h	H_2/air	Catalyst, Nafion layer on the CL, membrane	Franck-Lacaze *et al.* (2010)

CV is for cyclic voltammetry. Cases with two levels of current density or voltages correspond to cycled tests, the duration of each periods is given in the second column from the left. The gases indicated in the third column are for anode and cathode, respectively.

3.4 Poor humidification of the reacting gases

3.4.1 General comments and steady-state poor humidification conditions

It is well known that the best humidification conditions for long-term PEMFC operation have to correspond to a compromise: sufficient hydration of the membrane by both high current density of the cell and suitable humidification of the gases, while avoiding formation of liquid water in the GDL structure or the channels of the bipolar plate. The suitable water management depends on the properties of the cell component, for example, the membrane thickness (the diffusion rate of water varies with the reciprocal of the membrane thickness), and the operating conditions such as the stoichiometric factors (high excess in reacting gases can lead to drying of the fuel cell structures).

Too dry conditions are known to reduce the electrical conductivity of the membrane, in particular, for the PFSA-based polymers: the immediate consequence is increased ohmic losses in the cell. At the catalyst vicinity, the hydration of the thin ionomeric layer has also an effect on the kinetics of the electrode reactions. As a matter of fact, protons formed at the anode or consumed at the cathode have to be transferred efficiently from/to the catalyst cluster: thus, dry conditions in the fuel cell structure are also to hinder the electrode reactions, in particular, the oxygen reduction at the cathode (Zhang *et al.*, 2008). In contrast, excessive humidification of the reacting gases is to result in formation of liquid water, in particular, closer to the outlet: this is to modify the flow conditions in the bipolar plate channels and the GDL, and thus to impede the transfer of the reacting gases to the catalyst surface. Moreover, excess in liquid water can simply damage the catalytic layer by flushing out the catalyst particles as well as the carbon support particles. Surprisingly, examination of the published works in the area reveals that aging phenomena have often been investigated with fully humidified gases, that is, in the presence of liquid water, in particular, for appreciable current density and low stoichiometric excess.

The relevant literature often reports the occurrence of polymer thermal degradation. The word, which appears somewhat vague, usually covers mechanical and chemical degradation. Although temperature is the governing factor for thermal degradation, too low hydration of the cell increases its significance.

- The mechanical degradation concerns the reduced mechanical property of the polymer, in particular, in terms of its tensile strength. In relation to the reduction in water uptake, membrane thinning is often observed. For long-term operations, the mechanical cohesion of the MEA layers

can be severely damaged and significance delamination phenomena are often reported. Because of occurrence of the above facts, degraded membranes are more prone to failures, tears, or cracks.
- The chemical degradation occurring at low current density (Section 4.1) is amplified with low RH of the feed gases (Liu *et al.*, 2001); in addition, Chen and Fuller (2009) showed that at OCV the side-chain cleavage is privileged over the main chain unzipping with dry reacting gases.

Mechanical and chemical degradations of the membrane can be observed separately by specific techniques, as described in Section 2. However, they have common incidence as observed by the formation of pinholes which are actually caused by local degradation of the polymeric chain and excessive stress on the thinned polymeric sheet: this is directly visible by increase in the fuel crossover, as observed, for instance, by Wasterlain *et al.* (2010).

3.4.2 Periodic variations of the gas humidity

Typical tests conducted upon cyclic variations of the RH of the inlet gases are given in Table 4. Cycling the RH of the inlet gases has been often conducted with periods of time in the order of 1 min. At the end of each phase, steady-state conditions of humidity in the membrane bulk may not be perfectly attained, whereas steady behavior of the electrodes, including the thin ionomeric layer, is to be observed. Other tests were carried out with dry gas periods longer than 10 min, for which steady-state conditions can be expected. As a matter of fact, Kang and Kim (2010) showed that the transient change in the internal resistance in the cell could be observed for periods in the order of a few minutes and that the cell was running at steady state after 15–20 min. The longer-period tests conducted by Huang *et al.* (2012) can be considered as repeated operation at fixed humidity. However, contrary to pulsed currents or potentials for which the main degradation effect was caused by the oxidative conditions at the cathode for zero or low current density, in the case of gas humidification, the brutal change is to induce degradation of the MEA, in addition to the above phenomenon of membrane drying or the possible washing out of the catalyst: as a matter of fact, periodic change in inlet gas RH is the source of repeated shrinking/swelling of the PFSA-based polymer. This is not only to create additional stress in the polymer structure, favoring the increase in fuel crossover—in particular, for operation at OCV as recommended by DOE for evaluation of the mechanical degradation of membranes—by formation of local tears or pinholes, but also to affect the mechanical adhesion of the MEA layers, and local delamination of the layers under RH cycling has often been reported.

Table 4 Examples of aging investigations upon periodic variations of the relative humidity of the inlet gases

Relative humidity (RH)	Time variable	Gas fed	Current/voltage	FC components observed	Reference
0–100%	120–150 s	H_2/Air	0.6 V (*)	CL, creep deformation	Jao *et al*. (2010)
0–100%	1200–30 s	H_2/Air	0.8 A cm^{-2}	CL, fuel crossover	Kang and Kim (2010)
0–100%	600–2400 s	H_2/Air	10 mA cm^{-2}	CL, membranes, GDL	Panha *et al*. (2011)
0–62%,100–62%	16–8 h	Dry H_2/Air	0.3 A cm^{-2}	CL, membranes, GDL	Huang *et al*.
0–120%	120–120 s	H_2/Air	OCV	Membrane	DOE
0–150%	120–120 s	Air/Air	–	Membrane–MEA	Mathias *et al*. (2005)

The duration of each period (dry humid) is given in the second column from the left. The gases indicated in the third column are for anode and cathode. (*) in addition to the two phases with cycled RH, the cell was maintained at OCV for 30 s for each cycle.

Comparison of various sources of data could be done on the basis of the total, accumulated period of time for which the cell is fed with dry gases, regardless of the frequency of the cycling. Such a comparison relies upon two implicit assumptions: (i) operation with humidified gases induces negligible aging in comparison to periods with dry gas feed; (ii) the transient effects in the MEA such as membrane swelling and shrinking are also not accounted for here. The data reported in Table 3 can be considered for this purpose. Kang and Kim, with repeated 1200s operation with dry gases, observed significant degradation of the cell, with a 47.5% reduction in the cell performance after 1200 cycles, that is, after 400-h run with dry gases. The MEA collapse reported by Huang with far longer periods occurred after approximately 432h, with comparable MEAs. Although the degradation observed was not exactly the same, the two sources of data indicate that, for appreciable periods in the RH cycling, the transient effect of the cycling mainly related to repeated mechanical stress was little significant. In contrast, Jao observed a reduction in the cell performance in the order of 30% after 520 cycles (120s under dry conditions), which corresponds to only 17h with dry gases: the more rapid degradation was certainly due to the additional period at OCV in the three-phase cycle (Table 4), which may be the stronger effect of repeated mechanical stress at the membrane–electrode interface. Moreover, Mathias *et al*. (2005) working in air/air feeding conditions reported significant fatigue in the MEA structure after 4000 cycles, that is, approximately 67 total hours at dry conditions. Although no current passed in the cell in their experiments, comparison of their results with the data under longer-period cycling shows the significance of transient mechanical phenomena in this cycling mode.

3.5 Freezing effect

PEMFC operation under the freezing point of water can occur, for instance, in transported applications, in particular, in winter weather conditions. Contrary to the former types of aging for which programmed accelerated tests have been designed, most investigations published dealing with sub-zero temperatures describe either the degradation observed or developed techniques to avoid such degradation. Before examining the investigation tests for evaluation of this type aging, we would like to briefly remind the effects of freezing conditions.

In a PEMFC submitted to freezing conditions, the water contained in the membranes or condensed from the humidified gases is to freeze: this can occur for idle operations or during its transportation or storage, for instance, in winter nights. The ice formed can block passage of the reacting gases in the fuel cell structure, rendering its restart difficult or

impossible without external warming up of the cell before. Ice formation can occur not only in the millimetric structures of the cell, that is, in the gas ducts and manifold and the bipolar plates, but also in the GDLs and the catalytic layers (Borup and papers cited therein). Because ice formation is accompanied by increase in volume of water, mechanical damages are to be expected. Ice formation can also affect the polymeric structure of the membrane, in particular, for PFSA-based polymers (Cappadonia *et al.*, 1994; Siu *et al.*, 2006; Yoshida and Miura, 1992). Water in Nafion polymer is known to consist of three fractions: nonfreezing water, which remains liquid even at −120°C because of the very significant water–polymer interaction, the bound-to-freezing water contained in the polymer channels and whose appreciable interaction with the polymeric chain protect from freezing at temperature noticeably below 0°C, and free water with a freezing point at 0°C. Long-term operations under freezing conditions reduce the membrane conductivity (Borup *et al.*, 2007; Oszcipok *et al.*, 2005); moreover, should the access of the reacting gases to the catalysts be blocked by ice crystals, rapid degradation of the electrodes operated in a given current density is to be observed.

Freeze–thaw cycles, occurring, for instance, in transported applications without continuous warming of the fuel cell system in the night, are known to be the cause of violent degradation of the cell, as often reported by the regular degradation of cell performance (Guo and Qi, 2006) and reduction in the ESA along freeze/thaw cycles. The repeated phases of dilatation–compression during freezing, then of volume contraction in the thawing lapses, are to affect the properties of the Nafion-type polymer, in particular its water uptake. At the CL, the ionomeric layer can also be affected by freeze/thaw cycles. Whereas the morphology of the catalyst clusters is little sensitive to the temperature, the carbon support and the neighboring MPL undergo a weakening during freezing, together with a progressive change in contact angle and porosity. Finally, breakage of carbon fibers forming the GDL has also been reported. In addition to the above individual effects on the cell components, the most significant degradation effects of freeze/thaw cycles are probably the degradation of adhesion of the carbon and polymeric layers, essentially because of the mechanical forces exerted at the electrode–membrane interfaces or between the CLs and the MPL: occurrence of peeling and delamination phenomena has been reported in a number of relevant papers.

The importance of this degradation factor in the significant potential applications of PEMFC has been a great incentive to develop protocols to avoid such effects. In most cases, the solutions proposed consist in purging the cell with dry gases for a time period allowing appreciable drying of the membrane, before shutting down the system, so that the stress

induced by freezing of the residual water amount will be of little significance.

As expressed above, no ASTs have been designed with a real methodology to highlight the freeze/thaw effects: in most investigations, the cell is submitted to temperatures cycles, being shut down before the freezing phase, and then restarted upon warming up. Investigations have been performed considering different levels of operating variables:

- Freezing temperature can vary from −20 to −80°C or even below: very extreme temperatures may appear as allowing magnification of the freezing effects on the cell components, but will the data obtained be representative to ''regular'' freezing temperatures outside central Siberia or Antarctic area?
- Cycle duration is seldom indicated in papers and technical reports. However, contrary to other operating parameters such as current density or cell voltage, the duration of the freezing phase has certainly less impact on the cell degradation than the number of cycles imposed: main degradation phenomena are to occur during ice formation as additional mechanical constraints are suddenly applied to the various structures of the cell even though long-term storage under subfreezing conditions has also visible degradation effects.
- The RH of the inlet during the freezing period, as commented above.

As expressed by Borup *et al*. (2007) the only moderate consistence of published papers is caused by the diversity of fuel cell technology. In particular, the operating conditions applied for MEA preparation—temperature, pressure, period of time, etc.—or the process used for electrode manufacture, depending on whether the catalysts are directly deposited on the membrane or conversely on the MPL of the GDL.

3.6 The case of contaminants

PEM fuel cell in operation can be contaminated by both gaseous and ion impurities. Ion impurities can be present in the cell, either in the form of transition metal cations resulting from corrosion phenomena from the bipolar (metal) plates or the end plates—or anions, for example, fluoride, sulfate, and sulfonate species being formed by MEA degradation. Additional occurrence can be caused by external inputs of salts upon insufficient quality of the water supplied, being the source of chloride or carbonate anions, and sodium or calcium ions.

Ambient air which is to feed fuel cells in automotive applications can contain contaminants such as sulfur or nitrogen oxides issued from car or stake exhaust at parts per million levels. Hydrogen sulfide traces in air are originated from industry. In the anode side, hydrogen-produced

upstream of the stack by hydrocarbon reforming is to contain traces of carbon monoxide and far larger amounts of carbon dioxide produced quantitatively from the hydrocarbon feed. Traces of ammonia can also be formed from the coexistence of hydrogen and nitrogen at high temperatures in the partial oxidation reforming chamber. For the sake of possible reduction in the operating cost, it has been searched for at least two decades to operate PEM fuel cells without too extreme purification steps of the feed gases: cell components have been improved for their higher tolerance to a given contaminant. Other contaminant, for example, Si or metals, can be present by degradation of the sealing gasket.

Although ion and gaseous impurities have very different origins and natures, both can have negative impact on the membrane or the CLs through comparable mechanisms of action. In addition, the methodology developed in investigating cell degradation upon their presence can be common.

3.6.1 A brief introduction to degradation effects

The effects of contaminants on the electrochemical behavior of a PEMFC together with the reaction mechanisms involved have been described in review papers: readers are invited to refer for instance to the contributions of Borup *et al*. (2007), Cheng *et al*. (2007), Zamel and Li (2011) and Li *et al*. (2008).

3.6.1.1 Contamination by ions Anion species can poison to some extent the platinum-based catalyst, where most metal cations have a direct action on the ionomeric membrane through their preferential adsorption on the sulfonate group. The ion adsorption obeys the following equilibrium (Okada *et al*., 1999):

$$n\mathrm{H} - \mathrm{M} + \mathrm{A}^{n+} = \mathrm{AM}_n + n\mathrm{H}^+ \tag{5}$$

where M denotes the sulfonate group of the ionomer and A^{n+} is the metal cation. Ion adsorption can therefore be considered in theory as a reversible process. However, for divalent and trivalent cations, the strong adsorption renders the regeneration to H^+-form polymer difficult for physicochemical conditions compatible with fuel cell operation. The competitive ion exchange even in the presence of cation traces—at the parts per million level—has two main consequences: (i) the water uptake described by the isotherm of water sorption is affected by the presence of sorbed metal cations; (ii) the ionic conductivity of the metal-form ionomer is usually around one decade smaller than that of the original polymer so that the conductivity of the partially complexed membrane varies linearly with the molar fraction of metal cations in the polymeric chain (Okada *et al*., 2001; Kelly *et al*., 2005). In addition to the loss in conductivity of the membrane, some metal cations such as Fe^{2+} near the

cathode can react with intermediate hydrogen peroxide (Fenton's reagent) to form hyper reactive hydroxyl radicals:

$$Fe^{2+} + H_2O_2 \rightarrow Fe^{3+} + OH^- + OH \quad (6)$$

The trivalent ion further reacts with another peroxide molecule to peroxide radical (•OOH). Chain reactions involving the two radicals are known to degrade the polymeric chain, either at the side chain or at the carboxylic end group of the main skeleton, as revealed by the formation of F^-, fluorinated acids, and S-containing species (Collier *et al.*, 2006) in the water released by the cell. Fenton's reagent can be used in liquid phase as *ex situ* technique, in particular, for membrane degradation: for instance, the protocol developed by Kundu *et al.* (2008) consists in soaking the membrane in a 30% H_2O_2 solution with 16mg/L Fe^{2+} cations, with fresh solution every 12h.

3.6.1.2 Gas contaminants Gas contaminants present in air or hydrogen can degrade the cell performance. Although far from exhaustive, Table 5 summarizes the main degradation effects reported in the literature. The observed degradation can be little reversible, as with exposure to S-containing species, or more reversible, as observed with carbon oxides and nitrogen-containing species. Nevertheless, repeated exposures are to result in irreversible damage of the membrane or the CLs.

3.6.2 A first attempt in methodology

The tolerance of a PEM fuel cell can be evaluated by addition of a contaminant in the feeding gas stream and observation of its response along time. Changing back the feed stream with injection of neat hydrogen is to indicate on the reversibility of the degradation by the considered contaminant. In most papers, the degradation text is described with the values for the gas flow rate, the contaminant concentration and the exposure period of time, the cell current or its voltage together with the MEA features, namely, its geometrical area, the grade and the thickness of the polymer membrane, and the catalyst loading and composition—in the case of bi- or trimetallic catalyst formulations. However, for engineers, the simple description of the operating conditions and the results obtained, for example, 120mV reduction in the cell voltage at a fixed current density does not suffice for possible—even meager—interpretation. Improvement in the reported data has been allowed through indication of the mole amount of contaminant injected (Nagahara *et al.*, 2008; Soto *et al.*, 2003, for instance); some authors did investigate the effect of their concentrations and maintain constantly the contaminant quantity. Therefore, comparison of various papers published with the same contaminating

Table 5 Main degradation effects of typical contaminants

Contaminant	Effect	Mitigation	Reference
CO (in H_2)	Competitive adsorption of anode Pt sites impeding hydrogen adsorption. Visible effect from the ppm level	Oxidize adsorbed CO by air bleeding or higher potentials. Design more tolerant catalysts with other metals, for example, Ru to favor CO oxidation to CO_2	Divisek *et al*. (1998), Wagner and Schulze (2003), and Murthy *et al*. (2003)
CO_2 (in H_2)	Possible inhibition of the anode surface by CO traces formed by reverse water gas shift reaction	Same as for CO: design more tolerant electrode catalysts or favor CO oxidation by air bleeding or anode oxidation	De Bruijn *et al*. (2002) and Janssen (2004)
NH_3 (in H_2)	Ion-exchange NH_4^+/H^+ resulting in lower membrane conductivity and water uptake; same phenomenon in the ionomeric layer hindering oxygen reduction. H_2O_2 formation at the cathode. Possible damage of the anode catalyst	More efficient air treatment upstream of the cell. Reverse ion exchange with neat hydrogen	Uribe *et al*. (2002) and Halseid *et al*. (2008)
H_2S (in air)	Competitive adsorption of anode Pt sites impeding hydrogen adsorption. Strong effect from the ppm level	More efficient air treatment upstream of the cell	Shi *et al*. (2007)
NO_x (in air)	Slight adsorption of NO_2 on Pt sites at the cathode. Reduction to NH_4^+ which can complex the ionomer	More efficient air treatment upstream of the cell. Cyclic voltammetry	Mohtadi *et al*. (2004) and Yang *et al*. (2006)
SO_2 (in air)	Adsorption on cathode Pt sites and reduction to Pt–SO and then to Pt–S. Decomposition of the membrane. More significant effect than NO_x	More efficient air treatment upstream of the cell. Cyclic voltammetry or OCV with neat air can partly regenerate the MEA	Yang *et al*. (2006), Jing *et al*. (2007), and Nagahara *et al*. (2008)
H_2S (in air)	Adsorption on cathode Pt sites to form Pt–S species	Same as for SO_2	Nagahara *et al*. (2008)

substance is possible in terms of specific amounts of injected contaminants in mole per square centimeter for instance.

Consider now the global system of a fuel cell being contaminated upon injection of contaminants (Figure 4) present in the gas phase—the case of contaminated waters flowing in the cell structure can be derived straightforward. All mole amounts are expressed per unit area in this paragraph. A fraction of the contaminant flow is adsorbed or consumed through cell degradation, n^{cell}, the rest leaving continuously the cell

$$n^{\text{in}} = n^{\text{cell}} + n^{\text{out}} \tag{7}$$

One can define n_0^{cell} as the maximum amount of contaminant which can be adsorbed in the membrane, either adsorption on one electrode, or by complexation of the membrane: n_0^{cell} can appear as a contaminant capacity at the electrode or in the membrane bulk. Contaminant is introduced in excess only if

$$n^{\text{in}} > n_0^{\text{cell}} \tag{8}$$

However, this condition may not be sufficient for the following reasons:

- The transport and the transfer rates of the gas injected in the cell—or the liquid flow—can be insufficient to allow contaminant molecules to reach the MEA surface before their possible adsorption;
- The contaminant is adsorbed in the membrane structure or at the catalyst surface. The adsorption process is often considered as a fast process: this is true for adsorption on the Pt clusters, but membrane complexation by the contaminant can be partly controlled by mass transfer, either outside the MEA or in the porous structure. In addition, equilibrium exists between the gas and the denser phase in terms of coverage fraction θ for the catalyst or concentration C for the membrane, and the mole fraction in the gas: for the case of the simple Langmuir's law:

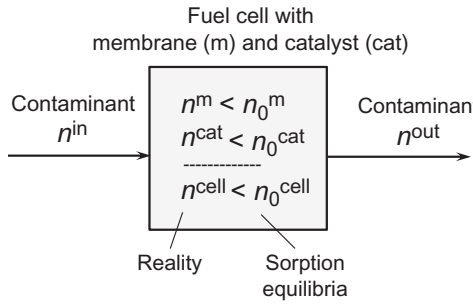

Figure 4 Contamination of a fuel cell with the various amounts of pollutant.

$$\theta = P\frac{ay}{y+b} \tag{9a}$$

$$C = P\frac{a'y}{y+b'} \tag{9b}$$

where P is the global pressure and parameters a, a', b, and b' characterize the adsorption equilibrium. Very strong adsorption corresponds to nearly full coverage fractions or saturation concentrations at low partial pressure of the gaseous contaminant.

Contamination capacity of the cell, n_0^{cell}, can be calculated with respect to the membrane, n_0^{m}, or the catalyst, n_0^{cat}, as follows:

$$n_0^{\text{m}} = \text{IEC}\, L_{\text{m}} \rho_{\text{m}} \tag{10}$$

$$n_0^{\text{cat}} = \frac{m_{\text{Pt}}}{M_{\text{Pt}}} \tag{11}$$

where IEC is the ion-exchange capacity of the membrane, L_{m} its thickness, and ρ_{m} its density, m_{Pt} denotes the Pt loading in the catalytic layer in milligram per square centimeter (only one electrode is considered here) and M_{Pt} the molecular weight of this element ($195.08\,\text{g}\,\text{mol}^{-1}$). Two examples are given below:

Nafion 112^{TM} membrane	$n_0^{\text{m}} = 9.19\,\mu\text{eq}\,\text{cm}^{-2}(*)$
Pt electrodes at $0.4\,\text{mg}\,\text{cm}^{-2}$	$n_0^{\text{cat}} = 2.04\,\mu\text{mol}\,\text{cm}^{-2}$

(*) for divalent cations, the capacity is to be two times lower.

Examination of the literature reveals that some investigations have been conducted with n^{in} lower than n_0^{m} or n_0^{cat}, and the contamination was therefore far from complete. In other reported cases, the inlet mole amount was nearly two orders greater than the contamination capacities, and it can be difficult to assess what could be the effect of lighter contamination on the state of health of the cell. A couple of literature examples are discussed in Section 4. Besides, because the cell is a reactor, with appreciable consumption of the reacting gas, variables y, C, and θ are to change in the cell, from the inlet to the outlet, resulting in uneven performance of the cell: this case will be briefly presented in Section 4 for the case of CO poisoning (Bonnet *et al.*, 2010).

4. LITERATURE EXAMPLES OF FUEL CELL AGING

This section presents published examples of PEM fuel cell aging: following the elements of methodology in Section 3, here are described typical aging phenomena, namely, the coupled degradation of the membrane and the CL upon oxidative conditions, the effect of poor hydration of the membrane, the specific case of bimetallic alloys, the effects of contaminants on fuel cell behavior and state, and aging upon start-up/shutdown procedures.

4.1 Coupled membrane and catalytic layer degradation

The degradation phenomena of the different components in operating fuel cells always occur simultaneously. Based on the general comments made in the previous section, this paragraph is aimed at describing the complex link between degradation phenomena of the membrane and the catalyst. The case of PFSA-based membranes and platinum catalyst is treated here.

4.1.1 Platinum dissolution

In the PEMFC operation, under highly oxidizing conditions such as operation at high cell voltage, feed with pure oxygen, and the presence of oxidants, for example, ozone or sulfur oxides in feed air, Pt catalyst dissolution can be considered as one of the most significant problems, which can cause FC performance loss. Among the possible reactions at each electrode, the degradation mechanisms of the electrocatalyst can be inferred from the following reactions (Pourbaix, 1966; Yu and Ye, 2007):

$$\mathrm{Pt} \leftrightarrow \mathrm{Pt}^{2+} + 2\mathrm{e}^{-}(\text{platinum dissolution}), \quad E_0 = 1.188\ \mathrm{V/NHE} \tag{12}$$

$$\mathrm{Pt} + \mathrm{H_2O} \leftrightarrow \mathrm{PtO} + 2\mathrm{H}^{+} + 2\mathrm{e}^{-}(\text{platinum monoxide film formation}), \quad E_0 = 0.98\,\mathrm{V/NHE} \tag{13}$$

$$\mathrm{PtO} + 2\mathrm{H}^{+} \leftrightarrow \mathrm{Pt}^{2+} + \mathrm{H_2O}(\text{chemical dissolution of platinum monoxide}) \quad \left[\log\left(\mathrm{Pt}^{2+}\right) = -7.06 - 2\mathrm{pH}\right] \tag{14}$$

$$\mathrm{PtO} + \mathrm{H_2O} \leftrightarrow \mathrm{PtO_2} + 2\mathrm{H}^{+} + 2\mathrm{e}^{-}(\text{formation of platinum dioxide}), \quad E_0 = 1.045\,\mathrm{V/NHE} \tag{15}$$

At the anode—lower potentials electrode—the solubility of platinum in acid is very low under the conditions of normal H_2/air PEMFC operation (Yu and Ye, 2007). At the cathode submitted to higher potentials upon exposure to air, PtO is produced by the reaction of Pt and O_2. The oxide is converted to Pt^{2+} by the reaction with dissolved H^+ in the water phase (or the ionomeric layer at the catalyst cluster). As briefly introduced in Section 2, platinum divalent cations can reduce back to metal at the surface of other clusters: whereas little Pt particles are prone to dissolve and disappear, others grow along the operation, representing Oswald's ripening phenomenon (Figure 2). Particle size distributions are to become broader, with a reduced active surface of the cathode as a consequence. Examples of size distributions are given in Figure 5.

Besides, Pt^{2+} ions can diffuse through the ion-exchange sites in the membrane bulk due to concentration effect or are transported by water

transport during the fuel cell operation. On encountering crossover H_2, Pt^{2+} can be reduced back to metal platinum and precipitate within the membrane as dispersed particles that comprise a metallic core and a shell of oxidized platinum (Péron *et al.*, 2008) forming sort of diffuse particle curtain in the polymer. Depending on the air and hydrogen compared stoichiometry, the location of the Pt particle layer is to vary, as evidenced by Guilminot *et al.* (2007a,b): for large excess of hydrogen fed to the cell, the back reduction occurs very soon after the dissolution and the particle curtain lies at a short distance from the cathode surface; on the contrary, the Pt particles are formed quite further in case of low hydrogen excess (Figure 6). Moreover, the significance of this phenomenon also depends

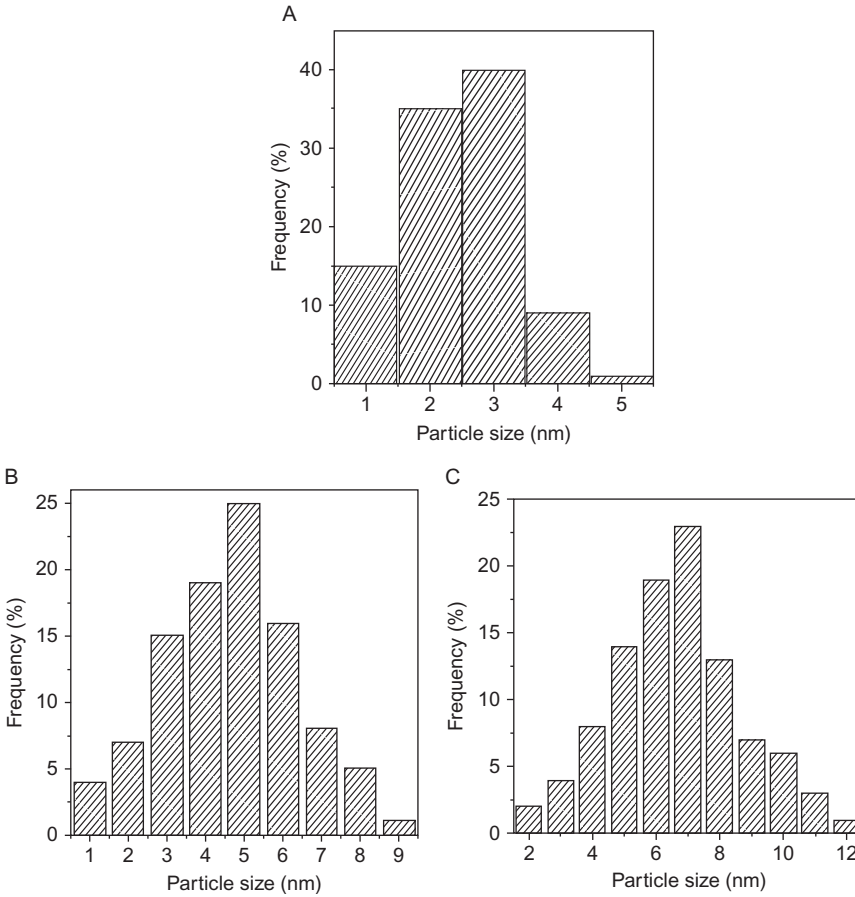

Figure 5 Examples of Pt crystal size distributions (a) fresh electrodes, (b) anode side after life test, and (c) cathode side after life test (Seo *et al.*, 2011).

on the fuel crossover, as expected. The Pt particles formed in the membrane reduce the proton conductivity of membrane by hindering water and ion transport through the hydrophilic part of the polymer structure.

4.1.2 Effects of Pt dissolution on membrane degradation

Platinum-charged species act as centers for the generation of free radicals as expressed by the following mechanism (Borup)

$$2H_2O_2 + Pt^{2+} \rightarrow 2HO^{\bullet} + 2OH^{-} + Pt^{4+} \quad (16)$$

$$H_2O_2 + HO^{\bullet} \rightarrow HO_2^{\bullet} + H_2O \quad (17)$$

For PFSA membranes, the small quantity of carboxylate end groups with H-containing terminal bonds, which are inevitably formed during the polymer manufacturing process, are regarded as the inducing agent for membrane chemical decay due to its susceptibility to radical attack. One generally accepts that in the mechanism the unzipping reaction initiates the abstraction of hydrogen from the end groups, which results in the releases of HF and CO_2 while forming new carboxylate groups at the chain ends: the following mechanism is usually considered (Borup *et al.*, 2007; Wu *et al.*, 2008; Zhang *et al.*, 2009a):

$$R_f - CF_2COOH + HO^{\bullet} \rightarrow R_f - CF_2^{\bullet} + CO_2 + H_2O \quad (18)$$

$$R_f - CF_2^{\bullet} + HO^{\bullet} \rightarrow R_f - CF_2OH \rightarrow R_f - COF + HF \quad (19)$$

$$R_f - COF + H_2O \rightarrow R_f - COOH + HF \quad (20)$$

The radical attack process can propagate along the main chain of the polymer membrane, and eventually the polymer decomposes into lower molecular fractions. Moreover, another decomposition reaction, namely,

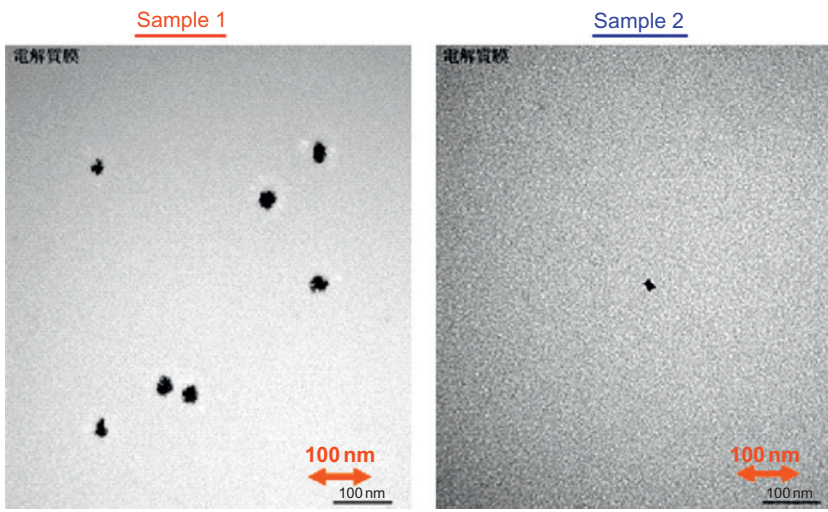

Figure 6 Pt particles formed in the Nafion membrane (Ohma *et al.*, 2008).

the side-chain cleavage, also occurs upon the action of OH• radicals as follows for the case of Nafion (Xie and Hayden, 2007)

$$-CF(COOH)-O-CF_2-CF(CF_3)-O-CF_2-CF_2-SO_3H+HO^{\bullet} \rightarrow -COOH+HOOC-CF(CF_3)-O-CF_2-CF_2-SO_3H+HF+CO_2 \quad (21)$$

The unzipping reaction eventually causes the main chain cleavage when it reaches the junction between the side chain and the main chain. As a result, the polymer main chain is cleaved and two carboxylic acid end groups are formed. Both mechanisms accelerate the chemical degradation of the membrane, namely, by reducing its thickness and leading to decrease in membrane proton conductivity and mechanical resistance. This latter induces the formation of failures, for example, tears, cracks, and pinholes.

4.1.3 Fuel (gas) crossover: An autocatalytic phenomenon

As described in the above paragraph, membrane aging can result from increasing gas crossover (hydrogen diffusion to the cathode). Highly exothermal direct combustion of hydrogen occurs on the catalyst surface and consequently generates local hot spots on the MEA. This can undoubtedly accelerate thermal degradation of the membrane and the catalytic layer (Borup *et al.*, 2007; Zhang, 2009b; Wu *et al.*, 2008), rendering more acute the fuel crossover. In addition, oxygen also diffuses the anode, with a rate estimated as being from one-tenth to one-half of the hydrogen flux, depending on the authors. Nevertheless, the presence in oxygen at the anode surface generates hydrogen peroxide, which is to form very active OH• radicals as explained in Section 4.1.2 and contribute to further degradation of the membrane. Finally, it is also believed that in the presence of Pt particles and H^+ cations in the membrane bulk, diffusing oxygen molecules can also form hydrogen peroxide, which is the source of oxidizing species (Figure 7).

4.1.4 Membrane creep formation

During PEM fuel cell operation, the MEA is submitted to compressive force between the GDLs. Under this constant compressive stress, PEMs undergo time-dependent deformation, such as creep (Solasi). Polymer creep can cause permanent membrane thinning and eventually failure (pinhole formation) and can promote entire fuel cell degradation compounded by chemical and physical degradation routes. Under normal fuel cell condition (with cell temperature below 80°C and hydrated condition), Nafion creep occurs at a slow rate, so catastrophic failure can take thousands of hours until the mechanical properties yield to the compressive forces (Borup *et al.*, 2007).

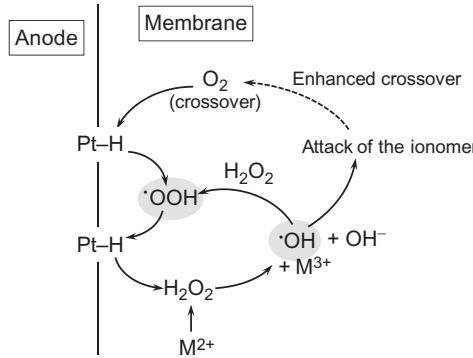

Figure 7 Formation of active species and radicals for the reduction of crossover oxygen, upon catalyst of metal cations (after Borup *et al.*, 2007).

Unfortunately, membrane creep deformation could accelerate catalytic layer degradation. For example, Jao *et al.* (2010) observed the increase in internal resistance and charge transfer resistance during RH cycling and suggested that this was caused by membrane creep formation. Kang and Kim (2010) highlighted that MEA delamination after RH cycling promoted the increase in both the internal resistance and the charge transfer resistance of the FC. In brief, membrane dimension change such as swelling/shrinkage due to RH change not only has an impact on the polymer mechanical resistance but also could affect the catalytic capacity of the fuel cell.

4.2 Effect of RH cycling, case of long periods

As expressed in Section 3.4, cycling the RH of the reacting gases between two levels at very low frequency corresponds to steady operation of the fuel with alternate hydration levels, with little incidence of the transient phenomena. The effects of the humidity low-frequency pulsation have been followed by Huang through three runs of a 25-cm^2 single cell (Huang *et al.*, 2012). For comparison with the run conducted at the nominal RH of the air stream at 62%, cycling was carried out either between 62% and 100% (high RH cycling) or between 62% and 0% (low RH cycling): the nominal RH value was maintained for 8 h, and the accidental period at 100% and 0%, respectively, was 16-h long. The MEA consisted of a 18-μm PFSA-based membranes with Pt/C cathode and Pt–Ru/C anode. For all tests, air and dry H_2 were fed to the cell at pressure close to the ambient level and temperature was kept at 55 °C. Stoichiometry of hydrogen and air oxygen was kept to 1.5 and 3, respectively. The variation of the cell voltage monitored until the MEA collapse exhibits very distinct profiles depending on the RH cycling (Figure 8).

4.2.1 Electrochemical behavior

Full humidification of air allows slightly higher cell voltages than the nominal level; sudden rises of the voltage in the profile were observed after determination of the fuel crossover or the electrochemical surface by cyclic voltammetry (Section 2). The average degradation rate of the cell voltage was near $12\,\mu V h^{-1}$, noticeably larger than that observed for the 1200-h-long reference test with RH=62% determined at $3\,\mu V h^{-1}$ (data not shown). The cell ohmic resistance r_{ohm} deduced from impedance measurements was little affected by the high RH pulsation (Figure 9): due to the water production in the cell, the cathode compartment was fully humidified in the main region of the cell. This resistance remained relatively constant along the 1500-h-long run, except after the electrochemical diagnoses, probably because of the temporary humidification of hydrogen. The charge transfer resistance for oxygen reduction, r_{ct}, exhibited regular increase, in consistence with the above cell voltage decay (Figure 10), also with little significant effect on the RH level. Between two electrochemical diagnoses, the degradation rate of r_{ct} was near 0.3% per day. However, because of the beneficial effect of these diagnoses, the average degradation rate was only at 0.12%, as for the test with constant RH=62%. For this cycling test, the fuel crossover increased slowly, regularly along time, attaining 2% of the operating current density.

Low RH cycling results in sharp pulsation of the cell voltage, with amplitude up to 90 mV; the run had to be stopped after 650 h (27 cycles). At nominal conditions, with 62% RH, the fuel cell exhibits a voltage decay

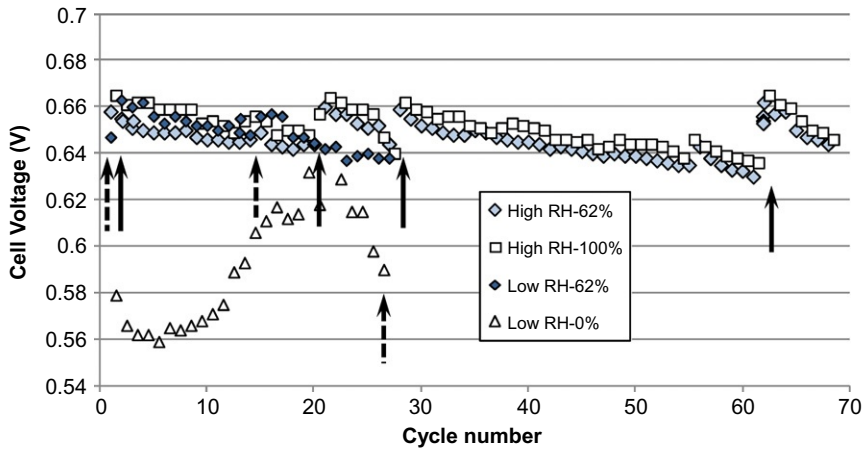

Figure 8 Cell voltage during the two RH cycling test. Arrows indicate the time for EAD and hydropgen crossover detemrination: solide arrow for the 62-100% RH cycling test, dorred arrows for the 62-0% RH cycling test.

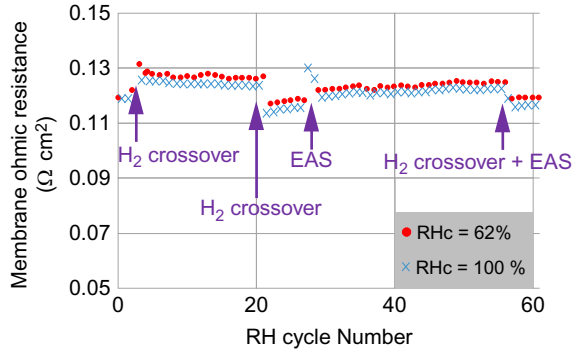

Figure 9 Resistances of the membrane (a) and the charge transfer for oxygen reduction (b) in the high RH cycling run (Huang *et al.*, 2012).

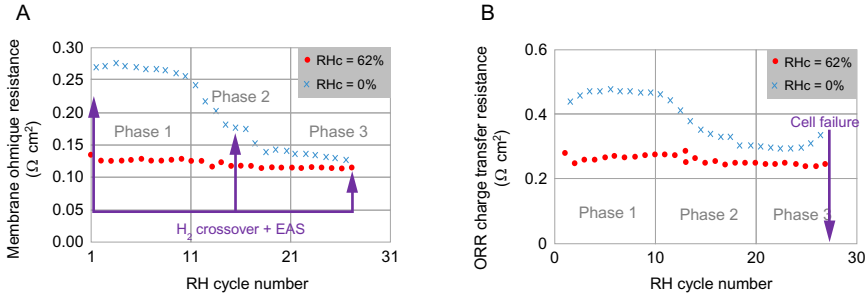

Figure 10 Resistances of the membrane (A) and the charge transfer for oxygen reduction (B) in the low RH cycling run (Huang *et al.*, 2012).

about $33\mu Vh^{-1}$. At accidental conditions (RH=0), the electrochemical behavior of the cell followed three phases:

- During the first 10 cycles—Period (1) in Figure 8, the cell voltage was nearly constant. In this period, resistances r_{ohm} and r_{ct} remained constant, approximately two times larger than their corresponding values at nominal humidification (Figure 10). Low cell hydration is detrimental to membrane conductivity and hinders oxygen reduction as explained in Section 2.
- In Period (2), the cell voltage increased regularly and tended to the value measured at nominal air humidification 62% RH; the two resistances r_{ohm} and r_{ct} decreased accordingly: this is likely due to the increase in fuel crossover allowing appreciable transport from the

anode to the cathode (data not shown), in particular, near the outlet of the cell, in a region where liquid water is formed because of the moderate hydrogen excess (λ_{H2}=1.5).

- After cycle 18, that is, in Period (3), significant water flow from the anode chamber and water production by oxygen reduction allow fair hydration of the cathode chamber, resulting in relative performance of the fuel cell: the cell voltage remained nearly 40 mV below with humidified air, and resistances r_{ohm} and r_{ct} were only 15% higher than those in the RH=62% periods (Figure 10). However, in the last four cycles, r_{ct} suddenly increased, before the MEA collapsed with negative voltage: before the collapse, the fuel crossover was estimated to approximately 100 mA cm^{-2}, that is, one-third of the operating current density, which explains occurrence of MEA end of life by hydrogen starvation.

EAS decreased linearly with time for both anode and cathode, for the reference run at constant RH and high/low RH cycling runs. The loss rate of the cathode EAS under high/low RH cycling was found to be 2–2.5 times larger than with constant RH; for the anode, the effect of high/low RH cycling is quite worse, with a loss rate around 3–4 times larger than in the reference test.

Considering the initial values for the EAS, the high RH cycling procedure induces a daily reduction in the EAS of 0.6% at the anode and 0.8% at the cathode. At the end of the run, the overall loss of EAS was 38% and 49% at the anode and the cathode, respectively. However, it can be observed that high RH cycling promoted significant EAS loss without significant effect on r_{ct} and the equivalent capacitance C_C (data not shown here). It can be estimated that $R_{ct,C}$ determined by EIS characterizes charge transfer capacity at the triple contact area, while the EAS determined by CV characterizes the electroactive sites on global CLs. Thus, these two features may not be perfectly correlated and may vary independently from each other.

For the overall low RH cycling test, the EAS loss was found to be at 27% at the cathode and 22% at the anode, corresponding to daily losses at 1.0% and 0.8%. The low RH cycling not only could accelerate the membrane degradation as revealed by the high crossover but also seems to accelerate the degradation of the catalytic layer. In fact, during low RH cycling, catalyst performance loss could be mainly due to carbon corrosion, since significance of carbon corrosion increases with low gas humidity and increasing potential (Borup). Loss of the carbon supporting the catalyst would cause detachment of nanoparticles from the carbon support which results in reduced EAS.

4.2.2 TEM observations

Compared to the membrane of fresh MEA, the MEAs aged under constant or cycling RH exhibit numerous bubbles and microholes formed throughout the membrane (Figure 11): as explained in Section 3, this may be caused by the chemical attack of peroxide radicals at the polymeric material. Bubbles and pinholes were formed in the middle of the cross-section of the membranes. As a matter, the Pt charged species formed by progressive dissolution of the catalyst act as locations for the generation of free radicals in the membrane bulk that chemically degraded the membrane (Péron *et al.*, 2008). Wang *et al.* (2008a) reported that the appearance of bubbles could originate from the decomposition of the polymer repeating units. The little voids formed from the polymer decomposition and the resulting pinholes are to make the membrane vulnerable to gas crossover. CL degradation in PEMFC during long-term operation includes cracking or delamination from the other layers. These various effects result from either the change in the catalyst morphology or loss of electrical contact with the active surface and can result in apparent activity loss of the CL. However, the severe delamination between the CL and membrane shown in Figure 11 could also have been caused by the TEM sample preparation process, as revealed similar tests with a fresh MEA.

Catalyst particle size distributions (Figure 12) were determined by TEM image analysis: examination of TEM images revealed the presence of catalyst agglomerates in addition to the ''regular'' particles, in particular, at the cathode: the agglomerates poorly resolved on the TEM images, and of irregular shape, were not taken into account for the determination of the distributions. MEA aging under constant air humidification led to larger catalyst particles.

After the high RH cycling, the particle size of the cathode catalyst tends to increase, exhibiting in addition a broader size distribution peak than in fresh MEA. This is mainly due to Pt nanoparticle agglomeration. At the anode side, particle size becomes slightly smaller which could be due to reduction of Ru to a more soluble form, such as hydrous Ru oxides before leaching out and crossing over to cathode, as reported by Cheng *et al.* (2007).

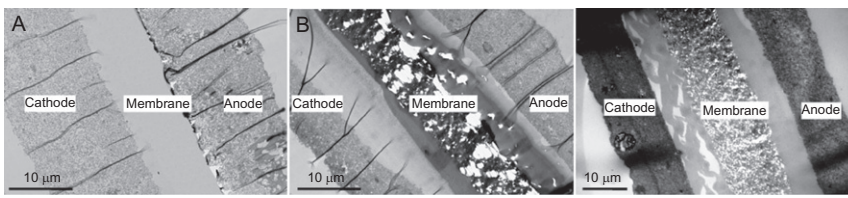

Figure 11 SEM view of the MEA before and after the with high RH cycling (center) and low RH cycling (right) long-term runs (Huang *et al.*, 2012).

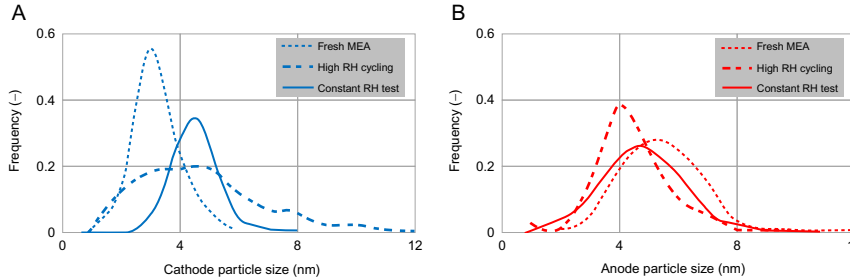

Figure 12 Size distribution of Pt catalyst deduced from TEM observations at the anode and the cathode (Huang *et al*., 2012).

For the low RH cycling, the distributions shown in Figure 13 reveal that in spite of the visible large agglomerates, the cathode catalyst particle size did not change significantly. As pointed out by Bi *et al*. (2007) transport of Pt ions formed by slow cathode dissolution is hindered in low hydration due to their lower diffusivity. This fact could restrain the significance of the often-observed process—Pt dissolution, ions migration then back reduction to metal Pt—leading to lower changes in the size distribution than with constant, nominal air humidification. In fact, the average size of catalyst particles at the anode was slightly lower at the end of the low RH cycling run than before (Figure 13): as expressed for the RH cycling, the likely dissolution of Ru from the anode is to explain the observed reduction in particle size. Nevertheless, the only moderate change in particle diameter during the low air RH cycling run—if one disregards the formation of agglomerates—is also caused by the restricted period of time in the low RH run, in comparison with the high RH cycling test.

4.3 Degradation of bimetallic alloy catalysts in PEMFCs

The major technological challenge in the development of highly active PEMFC catalysts relies in the ability to modify the structure at the nanoscale without altering their durability. At the present time, Pt-based catalysts are the most promising materials in terms of catalysis and durability for cost effective applications, but the high cost of Pt and its limited world supply prevent, in the current state of the technology, its wide-spread commercialization. To meet the requirements for large-scale automotive applications, two strategies must be developed. On the one hand, the Pt loading of MEA must be reduced significantly. Indeed, a specific Pt power density inferior to $0.2\,g_{Pt}/kW$ is required for financially viable applications which could be met by reducing MEA Pt loading to $0.15\,mg_{Pt}/cm^2$, so the cathode loading to $0.1\,mg_{Pt}/cm^2$ without loss of performance (Chen *et al*., 2010). On the other hand, highly active

electrocatalysts must be developed to enhance the electrochemical reaction rate, in particular, the ORR that controls the fuel cell performance.

4.3.1 A brief overview on bimetallic alloys

On the one hand, three types of cathode catalysts have been developed. The most commonly encountered one is the Pt catalyst supported on highly active carbon (Pt/C) or other support. This type of catalyst exhibits high catalytic activity for fuel cell reactions, but its high price and relatively low stability prevent its wide-spread utilization for automotive applications. Then, for the past few years, modified or nonmodified Pt-based catalysts have gained a renewed interest in academic and industrial research because of their lower cost and higher performance. They generally consist in a bimetallic alloy Pt–M (M being a transition metal) that can be chemically, physically, and/or electrochemically nanostructured to enhance its catalytic performance and/or durability. The use of another metal element in bimetallic catalysts allows reducing Pt loading within the MEA and so decreasing the overall cost of the PEM system. Moreover, catalysts such as Pt–Co, Pt–Ni, Pt–Fe, Pt–Cu, etc. exhibit two- to fourfold higher mass activity toward ORR compared to state-of-the-art Pt/C (Gasteiger *et al.*, 2005). Finally, nonprecious PEM catalysts mostly based on nitrogen-coordinated Fe or Co have also been investigated, but their performance are 150–200 mV below those achieved with Pt/C catalysts making them insignificant for PEMFC applications.

On the other hand, CO tolerant anode catalysts have been developed to allow using reformate hydrogen with minimum performance loss. Catalysts such as Pt–Fe, Pt–W, Pt–Mo, or Pt–Ru, the latter showing the best performance for hydrogen oxidation in the presence of CO, have been proposed (Pereira *et al.*, 2009).

4.3.2 Designing catalytic properties

Many excellent papers reviewing and/or investigating durability and catalytic properties of bimetallic catalysts have been published (Antolini *et al.*, 2006; Chen *et al.*, 2010; Mani *et al.*, 2011; Zhang *et al.*, 2009a,b). Among them, the general features can be expressed.

The enhancement of the catalytic properties of bimetallic catalysts is attributed to the change in the electronic structure of Pt: the ligand effect of the transition metal in the alloy induces a lattice contraction which increases the Pt d-band vacancy and decreases the Pt—Pt bond distance. The contracting effect, depending on the electronegativity of the second metal, becomes less pronounced with increasing number of Pt monolayers surfacing the alloy and becomes almost nil if their number exceeds four (Schlapka *et al.*, 2003).

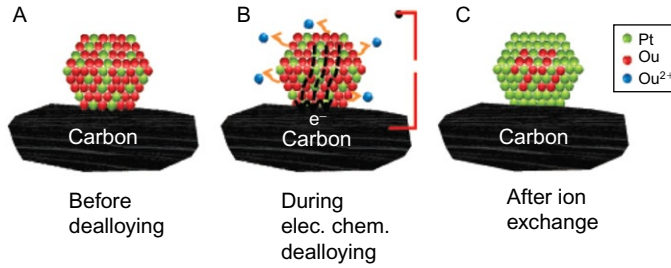

Figure 13 Scheme of electrochemical dealloying (Mani *et al.*, 2011).

So far, the highest ORR activities reported in PEMFC are obtained with electrochemically dealloyed Pt-alloys with high transition metal content (>50%, atm.). To achieve the dealloying step, the surfacing, less noble, transition metal is dissolved in the electrolyte (*ex situ*) by fast scan cyclic voltammetry (up to 1.2V/RHE) resulting in a ''core–shell'' structure. Figure 13 presents the scheme of the electrochemical dealloying process.

Other methods such as high-temperature annealing or acid leaching exist to obtain this type of structure.

4.3.3 Degradation

As pointed out by Chen *et al.*, conventional and dealloyed Pt-alloys/C offer effective higher catalytic performance, but the question whether their durability in PEMFC changing conditions (steady state, voltage/load cycling, etc.) will meet the requirements over the fuel cell life remains unanswered.

Under PEMFC potentials and acidic conditions, Pt-alloy/C catalysts are thermodynamically unstable: preferential dissolution of the less noble metal occurs, leading to a Pt-enriched surface. As mentioned before, Pt, also subjected to corrosion at high cathode potential, can dissolve and cause further underneath alloy exposure to the electrolyte again. Thus, depending on the diffusivity of the second metal within the alloy, chemical/electrochemical conditions in which the catalyst has been exposed together with its initial composition, changes in morphology and composition may vary. Thus, long-term aging may lead to different types of nanostructures. As an example, two pathways for PtCo catalysts degradation with different initial Co contents have been proposed (Chen *et al.*, 2010) (Figure 14). For stoichiometric alloy particles, dissolution of Co from the upper atomic layers of the particles leads to a Pt-skin or Pt-skeleton

structure on which dissolved Pt redeposits via Ostwald ripening. This leads to the previously described ''core–shell'' structure with a Pt-shell and alloy core. For alloys with higher Co content, percolated Pt_xCo than Pt-rich spongy particles are believed to be formed.

The behavior of second metal after dissolution depends on the thermodynamics and is often found to be a source of MEA contamination and performance degradation. Thus, contrary to Pt or Pd ions that are reduced by permeating H_2 into crystallites inside the membrane, cations such as Co^{2+} or Ni^{2+} are thermodynamically stable at low pH and the majority remains ion exchanged in the ionomer. Their stronger affinity with sulfonic groups than protons allows displacing them resulting in lower membrane proton conductivity, dehydration, higher membrane resistance, and lower ORR kinetics by a decrease of oxygen concentration or oxygen diffusion coefficient in the ionomer (Okada *et al.*, 2001 from Antolini *et al.*, 2006). Moreover, as discussed before, foreign cations greatly catalyze the formation of hydrogen peroxide radicals, responsible for the membrane chemical degradation (Inaba *et al.*, 2006). To reduce metal contamination, preleaching of the bimetallic catalyst has been proposed before PEMFC operation (Gasteiger *et al.*, 2005).

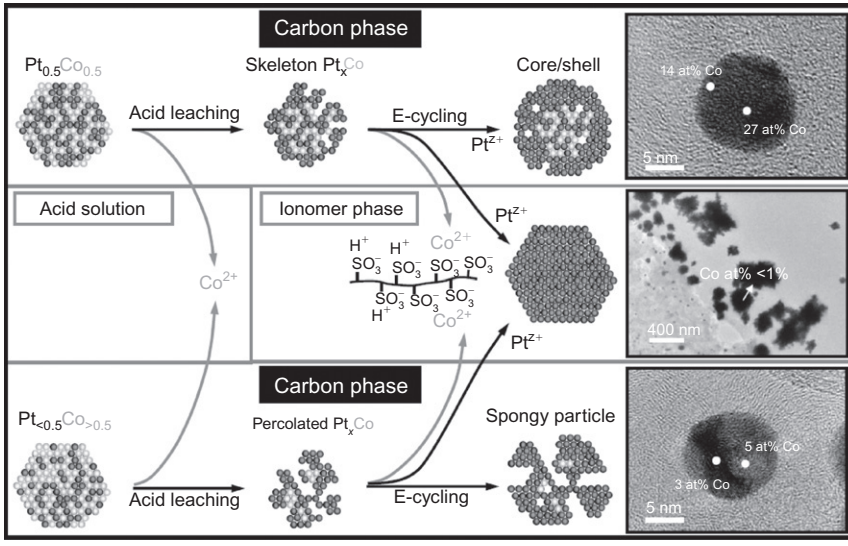

Figure 14 Pathways for Pt/Co degradation (Chen *et al.*, 2010).

4.3.4 Degradation evaluation

Diagnosis methods for the investigation of catalyst degradation have already been presented in this chapter, but for the case of bimetallic catalysts degradation, further details are worth mentioning.

First, CV profiles give useful information on the surface state of the catalyst, especially in the voltage range 0.05–0.4 V/RHE where underpotential deposition of hydrogen (H_{upd}) occurs. In particular, with bimetallic catalysts, CV profiles evolution gives qualitative insight of the decrease in the catalyst surface alloying degree. Thus, with fresh Pt-alloy/C catalysts, H_{upd} desorption peaks can be hardly distinguished and eventually form an overall broad peak (Figure 15). Besides, as the alloy surface enriches in Pt along the catalyst aging, H_{upd} peaks become sharper and CV profiles become more and more ''Pt like'' (Figure 15).

The second metal content in the alloy can be estimated by using different techniques:

- Assuming Vegard's law applies to the considered binary system, XRD analysis allows determination of alloy lattice parameter leading therefore to the second metal content within the catalyst (Dubau *et al.*, 2011).

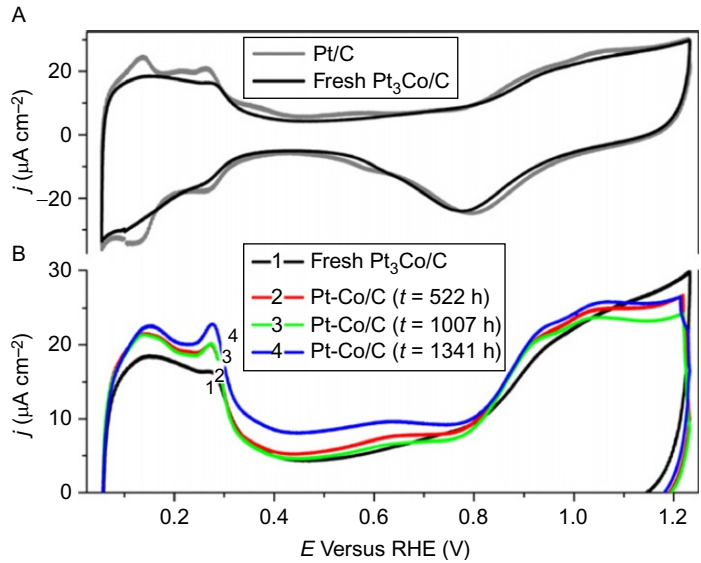

Figure 15 HUPD voltammograms of fresh or aged Pt_3/Co/C catalysts (Dubau *et al.*, 2010).

Compared to pure Pt, a shift in the higher degrees of the bimetallic alloy XRD patterns indicates a lattice contraction due to the incorporation of the second metal.
- Bimetallic alloy can be digested in Aqua Regia or other highly corrosive solution, and second element may be titrated by ICP-AES.
- X-ray energy dispersive spectroscopy (X-EDS) is used for chemical characterization of a sample. This technique may be performed on nanoparticle samples to determine the second metal content.

4.3.5 Future needs

The enhancement of the electroactivity of dealloyed catalysts compared to state-of-the-art Pt/C is established, but high activity is meaningless without high durability. If more fundamental works must be carried out to improve comprehension of the fundamental mechanisms that rule catalyst degradation, tests in real PEM conditions remain the ultimate criterion for catalyst evaluation. Yuan *et al.* (2011) reviewed the different durability test protocols available to investigate MEA long-term performance. To our knowledge, only one study on the durability of bimetallic catalysts exceeding 1000 h of PEM operation exists (Dubau *et al.*, 2010). It reports the formation of ''hollow'' Pt nanoparticles with an enhanced catalytic activity compared to the nonsegregated catalysts.

4.4 Examples of FC contamination

4.4.1 Analysis of published data

As expressed in Section 3, the mole amount of contaminant can be compared to the contamination capacities n_0^{m} and n_0^{cat} for possible assessment of the contamination extent, even in terms of inequality. A few published examples are given below.

- Kelly *et al.* (2005) reported the results of Nafion 117 contamination by dilute salts solutions. A membrane sample of 5.6 cm^2 was soaked in 50 cm^3 solution of metal transition salts with concentrations ranging from 0.1 to 100 ppm until equilibrium between the liquid phase and the polymer could be attained. Analysis of the membranes led to the amount of metal cations sorbed. Considering the membrane thickness (7‰), the ion capacity of the membrane can be estimated to 32.17 $\mu\mathrm{mol}\,\mathrm{cm}^{-2}$. Besides, the inlet mole number of Nickel cations—here contained in the solution volume—is calculated, using the molecular weight of nickel (58.7 $\mathrm{g}\,\mathrm{mol}^{-1}$). Then, this mole number can be expressed in terms of equivalent (because Ni^{2+} is a divalent species) and by surface area, leading to n_{in} values ranging from 0.0304 to 30.4 $\mu\mathrm{mol}\,\mathrm{cm}^{-2}$ for the above concentrations of nickel ions: in all cases, the membrane was not

saturated with the transition metal. Moreover, the data reported in Figure 1 of the quoted paper indicate that the weight amount of cations adsorbed in the membrane varied fairly linearly with the initial concentration in the liquid solution, being in addition close to the initial mass of Ni^{2+} introduced: this shows that Ni^{2+} is preferentially adsorbed on the membrane over H^+ species at all concentration levels, corresponding to a very steep sorption isotherm of the metal cation in the Nafion structure. Similar comment can be made for the two other metal salts investigated.

- Jing *et al*. investigated the effect of 1 ppm SO_2 and 1 ppm NO_x (80% NO_2, 20% NO) in an air stream on the electrochemical behavior of a 5 cm^2 PEMFC operated at 0.5 A cm^{-2}. The air stream was fixed at 600 cm^3 STP at 0.1 MPa, corresponding to a stoichiometric factor of air oxygen close to 14.4. Injection of the pollutants either separately or together in the air streams resulted in continuous, regular decay of the cell voltage during the 100-h-long run: the overall voltage loss was at 70 mV for NO_x and 130 mV for SO_2. The mole amounts of gases, n_{in}, can be calculated at n_{in}=32.14 µmol cm^{-2}. The MEA specifications (Nafion 212, with 0.5 mg Pt at the cathode) yielded n_0^m=9.19 and n_0^{cat}=2.55 µmol cm^{-2}. For both cases, excess in contaminant was fed to the cell: the amount of nitrogen oxide, which is expected to reduce to ammonium ions to adsorb on the ion-exchange polymer, exceeds the membrane capacity by a factor 4; the excess is far worse for the cathode catalytic layer to be inhibited by the sulfur dioxide. The only moderate effect of the two contaminants although fed in excess can be explained as follows.
  - From the sorption equilibria of NH_4^+ on Nafion, and of sulfur dioxide on Pt, the low content in contaminant in the air stream corresponds to only low values for coverage fraction θ in the polymer or at the Pt surface, respectively, for NO_2 and SO_2. However, in such case, the cell voltage would be expected to reach a steady value, expressing the sorption (or inhibition) equilibria either in the membrane or on the catalyst surface.
  - The high value for the air stream considered, corresponding to very low residence time in the 5 cm^2 cell, does not allow efficient sorption of the contaminants from the gas phase to the membrane or to the catalyst, so that gas and condensed phases are far from equilibrium. Additional tests with lower flow rates would indicate on the validity of the hypothesis.
- Although carried out with fixed stoichiometric factors, the experiments carried out by Mohtadi *et al*. (2004) with 2.5 ppm nitrogen dioxide or 5 ppm sulfur dioxide with stoichiometric factor of air oxygen at 2 led to nearly steady behavior of the fuel cell within shorter period of time: at the end of the runs, the inlet mole amounts were, respectively, at 2.69 and 5.15 µmol cm^{-2}. For the cell of interest provided with Gore 5621

membrane and 0.6 mg cm^{-2} Pt cathode, the membrane and catalyst contaminant capacity can be estimated at 6.43 and 3.06 μmol cm^{-2}, respectively. For NO_2 which was not introduced in excess, the current density at the end of the 24-h test attained was reduced by 58% from the initial level; for sulfur dioxide, for which n_{in} is larger than n_0^{cat}, the final current density was only at 20% of its initial value. Although contamination by the two oxides cannot be compared, the two results show that comparison of mole amounts n_{in} and n_0^{cell} may allow qualitative information on the cell degradation, for the considered operating conditions: this also lets appear that too large gas excess can affect the investigation of cell degradation by gas contaminants.

4.4.2 Another example: Nonuniform behavior of the cell under low stoichiometric factor for the case of CO poisoning

Inhibition of platinum surface by carbon monoxide, in particular, in PEMFCs has been largely investigated: significant effects of the contaminants on the cell voltage have been observed, with concentrations ranging from 1 to 100 ppm, depending on the operating conditions. As a matter of fact, because the cell can be considered as a reactor—with appreciable hydrogen consumption along the electrode surface, the gas composition is to vary in the cell from the inlet to the outlet. A 1D model has been proposed to predict the distributions of anode poisoning, overpotential and current density in a PEM fuel cell working at constant current density, depending on the hydrogen stoichiometric factor λ_{H2} (Bonnet *et al.*, 2010).

The 1D model uses the cell area S as the coordinate, varying from 0 at the inlet to S_{cell} at the inlet (Figure 16). The cell was assumed isothermal at 70 °C. Water transport from the cathode (with coefficient a_w) is accounted for, and the cell was modeled as a plug flow reactor.

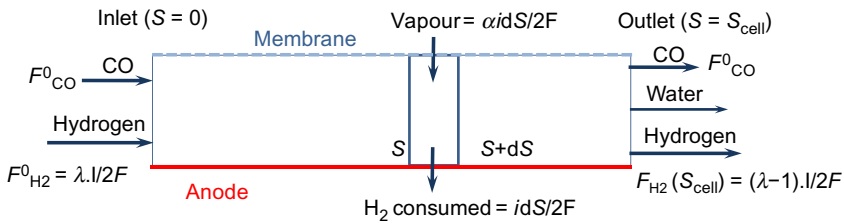

Figure 16 Principle of the 1D model for anode poisoning by Co containing in the hydrogen stream (Bonnet *et al.*, 2010).

Therefore, the overall flow rate in the anode chamber F_t can be written as:

$$N_t = N^0_{CO} + N^0_{H_2} - \int_0^S \frac{i(S)}{2F} dS + \alpha_w \int_0^S \frac{i(S)}{2F} dS \quad (22)$$

where the last term represents the mole flux of water produced at S. When the partial pressure of water reaches the saturation pressure, the excess of water condenses and the gas flow rate is calculated from F_t, taking into account the condensation phenomenon. The inlet hydrogen flow rate is obviously linked to the stoichiometric factor and the overall cell current as follows:

$$N^0_{H_2} = \lambda_{H_2} \frac{I_{cell}}{2F} \quad (23)$$

Besides, monoxide adsorption is described after the model developed by Bhatia and Wang (2004). Moreover, the current density for hydrogen oxidation was shown to obey the following law for the local current density:

$$i(S) = \frac{I_{cell}}{S_{cell}} = i_{0,a}\left(1 - \theta^0_{CO}\right)^2 \exp(b_a \eta_a) \quad (24)$$

where θ_{CO} is the coverage fraction of CO and η_a is the anode overpotential at S. Kinetic parameters had been found from previous experiments (Bonnet):

$$i_{0,a} = 1.2 \text{A cm}^{-2} b_a = 23 \text{ V}^{-1}$$

Finally, the expression for the cell voltage was used:

$$V = V_0 - r_{ohm} i - \eta_a - |\eta_c| \quad (25)$$

where r_{ohm} is the ohmic-specific resistance of the cell and η_c the cathode overpotential. The kinetic law for oxygen reduction considered here was also reported in Bonnet *et al*. (2010). Solving Equations (22)–(25) led to the distributions of current density, anode overpotential, and coverage fraction of carbon monoxide.

The results reported in Figure 17 below show the significant effect of the hydrogen stoichiometric factor on the unevenness of the distributions, for CO injected at 1 ppm in the hydrogen stream. For very large values of λ_{H2}, the gas composition is little changed from the inlet to the outlet of the fuel cell, the coverage fraction is little modified, so are the anode overpotential and the current density. Conversely, for λ_{H2}=1.1, that is, with 10% excess in hydrogen, the anode overpotential attains 0.212 V at the cell outlet—to be compared with 0.075 V at the inlet, corresponding to most uneven current density profiles in the cell. Considering higher CO concentrations in the inlet hydrogen amplifies the inhibition significance as expected, with also the impact of the stoichiometric factor on the unevenness of the various distributions. The overall model clearly demonstrates

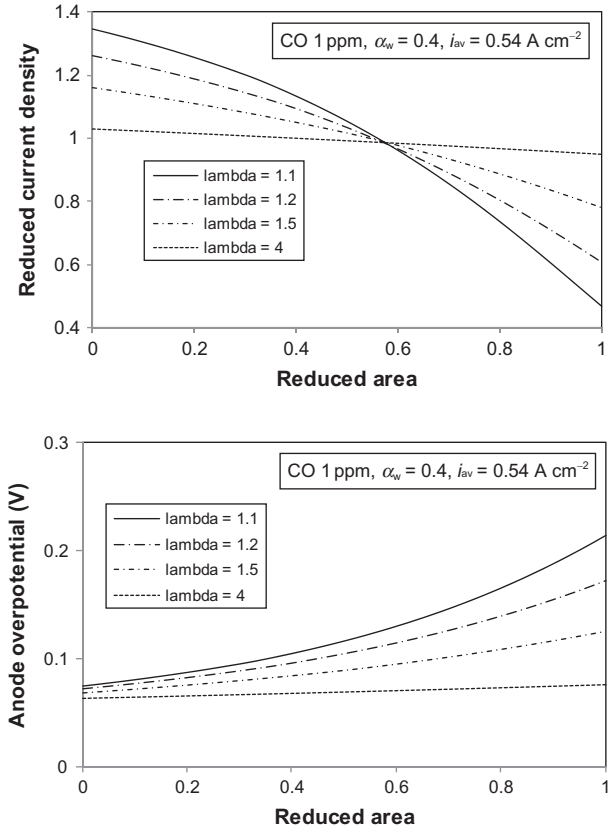

Figure 17 Effect of the stoichiometric factor of hydrogen on the distributions of reduced current density and anode overpotential in the fuel cell: predictions of the 1D model (Bonnet *et al.*, 2010).

that for practical operations, that is, when hydrogen is fed in low excess, the local performance of the cell varies greatly from the inlet to the outlet, which is to induce accelerated aging of the membrane and the cathode in regions with current density is far over its calculated average value: this phenomenon has also to be accounted for, while defining the operating conditions for an experiment campaign.

4.5 Aging by shutdown/start-up procedure

Opening the electrical circuit of the cell after operation results in large cell voltages—OCV—because of the presence of hydrogen at the anode and oxygen/air at the cathode: this is to be detrimental to the MEA, as discussed previously. Besides, introduction of air into the anode compartment, either by natural diffusion of air through the open inlet tubes or by forced injection of the gas, is to create a hydrogen/air boundary in the anode compartment, which results in accelerated degradation of the MEA, as evidenced by Reiser *et al.* (2005), then investigated by various authors. Now, consider the PEM fuel cell at equilibrium, with air in the two compartments: the cell voltage is zero. During the transient introduction of hydrogen into the anode chamber in the start-up procedure, a hydrogen front is formed, moving from the inlet to the outlet of the cell with comparable consequences as for the shutdown mentioned above. Similar situation of hydrogen-rich regions and hydrogen-starved regions of the fuel cells can also exist for maldistribution of hydrogen that may be caused, for instance, by transient blockages of the hydrogen flow in the anode compartment channels and with appreciable side-diffusion of air (or oxygen) from the cathode. This case considered by Reiser *et al.* (2005) and Meyers and Darling (2006) does not however correspond to well-defined hydrogen front, as it can be in start-up/shutdown operations.

The principle of the particular transient state of the cell has been investigated by various authors (Kim *et al.*, 2009; Maranzana *et al.*, 2010; Reiser *et al.*, 2005; Tang *et al.*, 2006) and presented in Yousfi-Steiner *et al.*'s (2009) review. The potential damage caused by the existence of a hydrogen front can be explained by comparing two situations at OCV as follows:

- In a normal fuel cell fed with hydrogen and oxygen—air—the highest potential at the cathode is near 1V or slightly below. For such conditions, Pt catalyst dissolves at a finite rate to Pt^{2+}, whereas carbon corrosion also occurs:

$$Pt \leftrightarrow Pt^{2+} + 2e, \quad E_0 = 1.118 \text{ V/NHE} \tag{26}$$

$$C + 2H_2O \leftrightarrow CO_2 + 4H^+ + 4e, \quad E_0 = 0.207\text{V/NHE} \tag{27}$$

Kinetics of reaction (27) is sluggish, so its significance could be neglected for potential below 1V. Nevertheless, the presence of Pt species is known to greatly catalyze carbon corrosion: therefore, for PEMFC's held for long periods at high voltage, that is, at zero current, or with very low current densities, both carbon and platinum in the cathode CL are to corrode, as discussed more in details in Section 4.1.

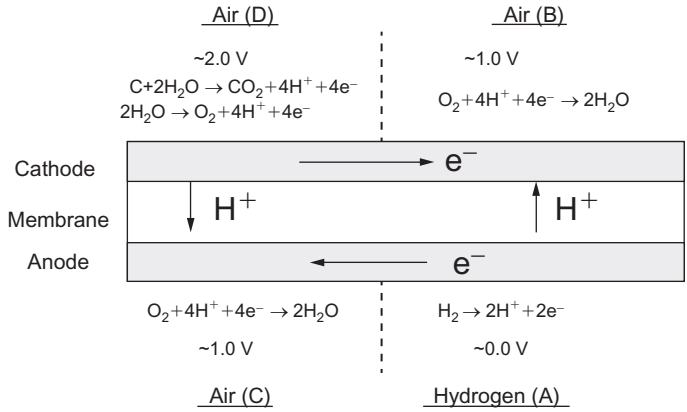

Figure 18 Introduction of hydrogen into the anode previously fed with air: transient existence of two cells with different reactions: dual cell configuration (Tang *et al.*, 2006).

- In the presence of air in part of the anode chamber, as shown schematically in Figure 18, the cell can be considered as consisting of two cells where anode and cathode are the place of different reactions, as follows. The anode part fed with hydrogen has a potential of 0 V, the facing part of the potential being at potential equal to OCV, that is, near 1 V, corresponding to oxygen reduction. The other part of the anode being hydrogen starved has also a potential near 1 V, corresponding to oxygen reduction to water. The overall current between anode and cathode is zero, but an internal current circulates through the anode because of the potential gradient and the high conductivity of the anode structure. Finally, because the cell current is to be uniform, the second part of the cathode, facing the O_2-containing anode chamber, is set to a potential which is nearly twice as large as the OCV, that is, near 2 V. Along time, as the hydrogen—or the air—front progresses to the outlet, the cell turns back to its normal configuration with a potential either zero—or at OCV, respectively—and the internal current decays. The principle of a variable front, with coupled time and space effect, is familiar to chemical engineers as in chromatographic or ion-exchange columns, for instance, allowing them easier representation of the phenomenon.

Investigations of PEMFC under such transient conditions have been conducted using both theoretical and experimental approaches: the published results can be described and commented through various aspects as follows.

4.5.1 Measurement of electrode potential and qualitative consequences

Dynamic hydrogen electrodes installed as a reference electrode in the PEMFC by Kim *et al*. (2009) to measure the individual cathode potential along time: when air flows into the anode channels filled with hydrogen, the cathode potential increases up to 1.4 V before decreasing down to near 1 V, and the cell voltage declines to zero when the anode channels are totally filled with hydrogen. Using another technique, Tang *et al*. (2006) showed that the cathode potential of the air-fed part of the cell was about to about 1.75 V versus the hydrogen-rich anode. In both cases, although below the theoretical value near 2 V, the cathode potential was shown to be large enough for efficient Pt oxidation according to:

$$\mathrm{Pt} + x\mathrm{H_2O} \leftrightarrow \mathrm{PtO}_x + 2x\mathrm{H}^+ + 2x\mathrm{e} \quad (28)$$

$$\mathrm{Pt} + x\mathrm{PO_2} \leftrightarrow \mathrm{PtO}_{2x} \quad (29)$$

the last oxide being prone to dissolution to Pt (IV) in acidic media. Carbon corrosion and water electrolysis are also to occur. As explained in Section 4.1. platinum ions generated from the cathode accelerate the decomposition of the membrane, at least for perfluorosulfonic polymers; in addition, the existing hydrogen crossover allows reduction of Pt ions in the membrane, resulting in the formation of Pt particles in the polymeric membrane (see Section 4.1), as reported by Meyers.

4.5.2 Electrical phenomena during start-up/shutdown procedures

Most of the published works in the area rely upon the concept of dual cell configuration, with the transient existence of two connected cells, an ammeter allowing evidence of the internal current mentioned above. Following global approaches of the transient phenomena, Maranzana *et al*. (2010) developed and used a segmented electrode in a dedicated fuel cell (Figure 19) to highlight coupling between time and distance from the gas inlet.

The 30-cm cell was formed by two bipolar plates with five linear channels being 0.7×1 mm in section. The anode plate was an aluminum plate coated with gold, whereas the cathode plate was machined out of polycarbonate and provided with segmented current leads: twenty 15×1-mm gold-coated brass strips were fixed on each of the four ribs. At the same axial coordinate, the four brass strips were connected to each other outside the cell. Rectangular GDLs and a nonsegmented MEA were installed to form the (cathode) segmented fuel cell. The 20 electrode segments were connected to the same potential and a 5-mΩ resistor allowed measurement of the current passing through each segment. Care was taken so that most of the current generated circulates through the wire and not from one rib to another by bypass through the GDL. The cell was tested for start-up procedure at OCV after N_2 or air filling in

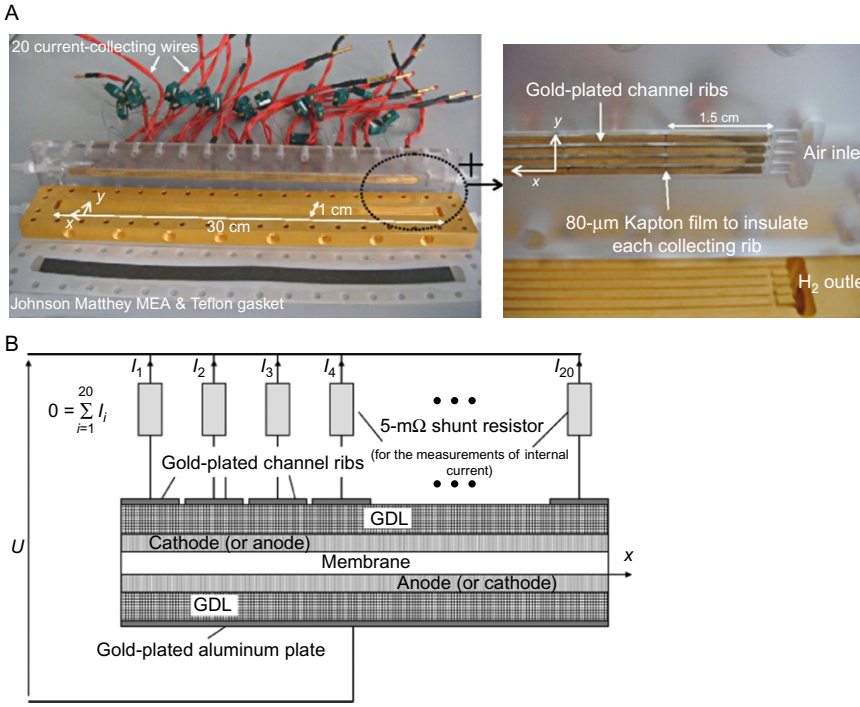

Figure 19 Segmented cell for investigation of transient (top, left and right) behavior of the cell in start-up(bottom) operation (Maranzana *et al*., 2010): (a) Photos of the cell and (b) electrical connections.

the anode chamber. After introduction of hydrogen to the cell, positive currents flow through the first segments, and because the overall cell current is to be zero, negative currents circulate the other segments further from the outlet. Figure 20 gives an example of current transient in the segmented cell. For the case of nitrogen-filled anode, the negative current corresponds to charging of the electrode segments, as first suggested by Siroma *et al*. (2006). For air-filled anode, the presence of oxygen allows occurrence of faraday processes, for example, carbon corrosion or even oxygen evolution in addition to the capacitive current.

4.5.3 Qualitative assessment of cell degradation upon shutdown/start-up cycles

Kim analyzed the gases emitted by the cell submitted to start-up procedure by FT-IR while measuring the cathode potential: he then could evidence the presence of carbon dioxide, carbon monoxide—for cathode potentials larger than 1.2V—and traces of sulfur dioxide, the origin of

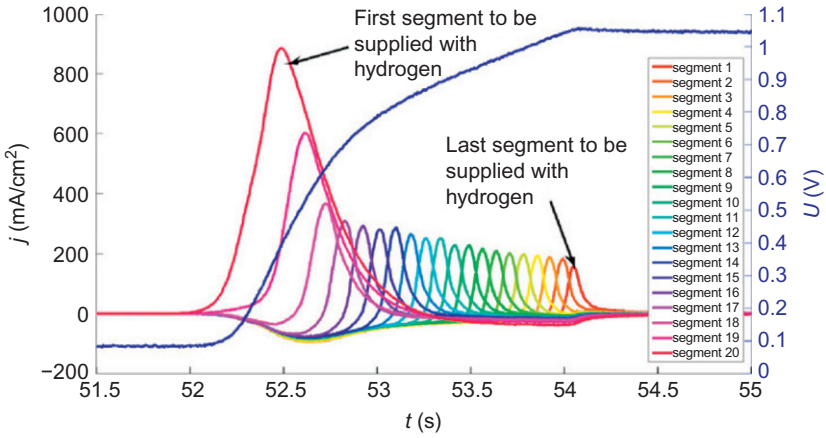

Figure 20 Current transients in start-up operation of the segmented cell (Lamibrac *et al*., 2011).

which could not be precisely highlighted. The external corrosion current measured was estimated by Meyers to be approximately one-half of the total corrosion current, whose density is in the order of a few milliampere per square centimeter. According to Meyers, the carbon corrosion current is limited to moderate values only by significant adsorption phenomena obeying Langmuir's isotherm for potentials below 1.1V.

Thickness of the cathode was measured by Kim from field emission scanning electron microscopy images (FE-SEM) to decrease from 13μm down to 5μm after 12 shutdown/start-up cycles. As also observed by other investigators, the anode was little affected by the series of cycles. Tang reported a two-third thickness reduction after 80 cycles, and the ESA estimated by voltammetry was found to be reduced by 80% in the meanwhile. Actually, comparison of the two sources of data is not straightforward, in particular, because the significance of these side-oxidation processes is as large as the gas flow rate in the anode chamber is low, as demonstrated by Lamibrac *et al*. (2011) by both measurements of the charge passed and determination of the carbon loss from the cathode. The significant decrease in cathode thickness and ESA reported in the literature are due to Pt oxidation/dissolution and to carbon corrosion: analysis of the impedance spectra confirmed the fact as revealed by reduced capacitances and large charge transfer resistances—in particular, in the first segments from the gas inlet. However, the above values for the cathode thickness or its ESA probably do not correspond exactly to the extent of carbon and Pt corrosion: as supposed previously in the chapter, the cathode morphology likely suffers from

compaction during the aging process, and the platinum clusters are submitted to change in their size by various mechanisms, for example, Ostwald ripening. Besides, slight but visible thinning of the membrane was also reported, in particular, by Tang: as for other modes of MEA degradation, the presence of Pt ions is to catalyze the decomposition of polyfluorosulfonic membrane. Once more, membrane thinning may be partly due to more compact morphology of the polymer related to reduced water uptake, in addition to the likely loss of polymer by unzipping reaction or side-chain cleavage: combination of these phenomena results in larger high-frequency resistance of the segmented cells (Lamibrac *et al.*, 2011).

5. SUMMARY AND CONCLUSIONS

Following four chapters devoted to the engineering description of the principles and the potentials of various types of fuel cells, the chapter has been focused on aging phenomena in fuel cells, more precisely on PEM fuel cells. Better understanding of the degradation processes occurring in the various parts of PEM fuel cells allows the hurdles of the energy conversion technology to be identified, which is to render possible the development of more efficient, more reliable fuel cell components.

In the present time, the development of fuel cell technology in the field of energy conversion is hindered by the high cost of cells together by their durability. This latter factor is still insufficient in most cases to render fuel cell technology perfectly competitive for large-scale commercialization. Nevertheless, cheaper fuel cells—benefiting from cheaper technologies for the manufacture of bipolar plates or from lower amounts of platinum in the electrodes—and offering higher energy efficiency—afforded by thinner membranes and more efficient catalytic layers—could be developed and introduced into specific market domains. However, these recent, more sophisticated components may sometimes be more fragile from the mechanical point of view to exhibit appreciable dissolution of the catalyst material from the electrode structure: their overall durability may not be significantly increased in spite of the technological improvements in the manufacture of the MEA. Impressive progresses in design and manufacture of fuel cell components certainly have been made for the two past decades, but some more have still to be made to reach the necessary compromise between performance and durability.

Aging of PEM fuel cells is known to be accelerated by idle operation, or upon cycling of various variables such as current density or gas feeds, presence of contaminants in the feed gases, repeated shutdown and start-up, or operations under freezing conditions. Damage induced

by the various aging modes can be of mechanical or chemical natures. For the first type of damage, the mechanical properties of the membrane and electrodes together with their mechanical cohesion seriously affected, whereas the chemical degradation often corresponds to oxidative decomposition of the ionomeric membrane or appreciable dissolution of the catalytic layer, that is, metal catalyst and/or its support.

Aging phenomena has to be considered as a whole in investigation of fuel cells either under operation or in postmortem analysis. The various examples given show that actually the damage is seldom the fact of a single component of the cell but in most cases concerns the degradation of the catalyst. As a matter of fact, dissolution of platinum, for instance, is known to have a significant impact on the ionomeric membrane, in addition to delamination issues.

In addition to the description of potential degradation and damage observed, we tried to present in this chapter first attempts in assessment of the damage significance, in particular, for the case of contaminants. The simple comparison of the contaminant amounts in the gaseous feed to the capacity of contaminant tolerance can be the first approach to be considered even though it is far from sufficient: more complete calculations have to be carried out. For this purpose, adsorption isotherms and kinetics, plus the reaction rates between contaminants and the active functions of the cell components, have to be integrated in the modeling, provided that the values of the various physicochemical data involved are available. Also in the comparison of published results of one specific degradation phenomenon to one's own data, care has be to be taken in the comparison of all operating conditions, in addition to the nature of fuel cell components. Finally, along this chapter, emphasis has been put on the complementary approach between material sciences and engineering sciences—in particular with the input of technological aspects, flow phenomena, transfer phenomena, or reactor modeling—for effective investigations of this complex, promising tool for energy conversion in view to its improvement.

LIST OF SYMBOLS

LATIN LETTERS

A, a'	coefficient in Langmuir's law, Pa^{-1} and $mol\,m^{-3}Pa^{-1}$
b	Tafel coefficient, V^{-1}
b, b'	coefficient in Langmuir's law
C	concentration, mole m^{-3}
D	diffusion coefficient, m^2s^{-1}

F	mole flow rate, $\mathrm{mol\,s^{-1}}$
F	Faraday's constant, 96,487 $\mathrm{A\,seq^{-1}}$
i	current density, $\mathrm{A\,m^{-2}}$
I	current, A
I_0	exchange current density, $\mathrm{A\,m^{-2}}$
IEC	ion-exchange capacity, $\mathrm{eq\,kg^{-1}}$
L	characteristic length, m
L_m	membrane thickness, m
m	weight, kg
M	molecular weight, $\mathrm{kg\,mol^{-1}}$
n	mole number, mole
N	mole flow rate, $\mathrm{mol\,s^{-1}}$
P	pressure, Pa
r	specific resistance, $\mathrm{Ohm\,m^2}$
S	geometrical area, $\mathrm{m^2}$
t	time, s
T	temperature, K
V	voltage, V
x	coordinate, m
y	mole fraction in the gas phase

GREEK LETTERS

α	water transfer coefficient
α	thermal diffusivity of the fluid (in Equation (4)), $\mathrm{m^2\,s^{-1}}$
η	overpotential, V
λ	stoichiometric factor
θ	coverage fraction
ρ	density, $\mathrm{kg\,m^{-3}}$
τ	characteristic time, s

SUBSCRIPTS AND SUPERSCRIPTS

0	initial or intrinsic conditions
a	anode
c	cathode
cat	catalyst
cell	cell
CO	related to carbon monoxide
$\mathrm{H_2}$	hydrogen
inlet	inlet conditions
m	mass transfer

m	membrane
ohm	related to oXhmic phenomena
outlet	outlet conditions
w	water

REFERENCES

Ahn, S.-Y., Shin, S. J., Ha, H. Y., Hinge, S.-A., Lee, Y.-C., Lim, T. W. and Oh, I.-H., *J. Power. Sources* **106,** 295 (2002).

Antolini, E., Salgado, J. R. C. and Gonzalez, E. R., *J. Power. Sources* **160,** 957 (2006).

Avasarala, B., Moore, R. and Haldar, P., *Electrochim. Acta* **55,** 4765 (2011).

Bhatia, K. K. and Wang, C. Y., *Electrochim. Acta* **49,** 2333 (2004).

Bedet, J., Maranzana, G., Leclerc, S., Lottin, O., Moyne, C., Stemmelen, D., Mutzenhardt, P. and Canet, D., *Int. J. Hydrogen Energy* **33,** 3146 (2008).

Bi, W., Gray, G. E. and Fuller, T. F., *Electrochem. Solid-State Lett.* **10**(5), B101 (2007).

Bonnet, C., Franck-Lacaze, L., Ronasi, S., Besse, S. and Lapicque, F., *Chem. Eng. Sci.* **65,** 3050 (2010).

Borup, R.L, Davey, J. R., Garzon, F. H., Wood, D. L., Welch, P. M. and More, K., *ECS Trans* **3**(1), 879 (2006).

Borup, R., Meyers, J., Pivovar, B., Kim, Y. S., Muikundan, R., Garland, N., Myers, D., Wilson, M., Garzon, F., Wood, D., Zelenay, P., More, K., Stroh, K., Zawodzinski, T., Boncella, J., McGrath, J. E., Inaba, M., Miyatake, K., Hori, M., Ota, K., Ogumi, Z., Miyata, S., Nishikata, A., Siroma, Z., Uchimoto, Y., Yasuda, K., Kimijima, K. and Iwashita, N., *Chem. Rev.* **107,** 3904 (2007).

Cappadonia, M., Erning, J. W. and Stimming, U. J., *Electroanal. Chem.* **376,** 189 (1994).

Chen, C. and Fuller, T. F., *Polym. Degrad. Stabil.* **94,** 1436 (2009).

Chen, G. B., Zhang, H. M., Ma, H. P. and Zhong, H. X., *Int. J. Hydrogen Energy* **34,** 8185 (2009).

Chen, S., Gasteiger, H. A., Hayakawa, K., Tada, T. and Shao-Horn, Y. J., *Electrochem. Soc.* **157,** A82 (2010).

Cheng, X., Shi, Z., Glass, N., Wang, L., Zhang, J. J., Song, D. T., Liu, Z. S., Wang, H. J. and Shen, J., *J. Power. Sources* **165,** 739 (2007).

Cleghorn, S. J. C., Mayfield, D. K., Moore, D. A., Moore, J. C., Rusch, G., Sherman, T. W., Sisofo, N. T. and Beuscher, U., *J. Power. Sources* **158,** 446 (2006).

Collier, A., Wang, H. J., Yuan, X. Z., Zhang, J. J. and Wilkinson, D. P., *Int. J. Hydrogen Energy* **31,** 1838 (2006).

De Bruijn, F. A., Papageorgopoulos, D. C., Sitters, E. F. and Janssen, G. J. M., *J. Power. Sources* **110,** 117 (2002).

Divisek, J., Oetjen, H. F., Peinecke, V., Schmidt, V. M. and Stimming, U., *Electrochim. Acta* **43,** 3811 (1998).

Dixon, D., Wippermann, K., Mergel, J., Schoekel, A., Zils, S. and Roth, C., *J. Power. Sources* **196,** 5538 (2011).

Dubau, L., Maillard, F., Chatenet, M., Guétaz, L., André, J. and Rossinot, E., *J. Electrochem. Soc.* **157,** B1887 (2010).

Dubau, L., Durst, J., Maillard, F., Guétaz, L., Chatenet, M., André, J. and Rossinot, E., *Electrochim. Acta* **56,** 10658 (2011).

FCtestnet: Fuel cell Testing and STandardisation thematic NETwork, http://www.jrc.nl/fctestnet/.

Ferreira, P. J., Ia O', G. J., Shao-Horn, Y., Morgan, D., Makharia, R., Kocha, S. and Gasteiger, H. A., *J. Electrochem. Soc.* **152,** A2256 (2005).

Franck-Lacaze, L., Bonnet, C., Choi, E., Moss, J., Pontvianne, S., Poirot, H., Datta, R. and Lapicque, F., *Int. J. Hydrogen Energy* **35,** 10472 (2010).
Garland, N. L., Benjamin, T. G. and Kopasz, J. P., *ECS Trans.* **11**(1), 923 (2007).
Gasteiger, H. A., Kocha, S. S., Sompalli, B. and Wagner, F. T., *Appl. Catal. B Environ.* **56,** 9 (2005).
Guilminot, E., Corcella, A., Charlot, F., Maillard, F. and Chatenet, M., *J. Electrochem. Soc.* **154,** B96 (2007a).
Guilminot, E., Corcella, A., Chatenet, M., Maillard, F., Charlot, F., Berthomé, G., Iojoiu, C., Sanchez, J. Y., Rossinot, E. and Claude, E., *J. Electrochem. Soc.* **154,** B1106 (2007b).
Guo, Q. H. and Qi, Z. H., *J. Power. Sources* **186,** 1269 (2006).
Halseid, R., Heinen, M., Jusys, Z. and Behm, R. J., *J. Power. Sources* **176,** 435 (2008).
Huang, B.T., Chatillon, Y., Bonnet, C., Lapicque, F., Leclerc, S., Hinaje, M., Rael S., Part I and 2, to be published in *Fuel Cells* (2012).
Inaba, M., Kinumoto, T., Kiriake, M., Umebayashi, R., Tasaka, A. and Ogumi, Z., *Electrochim. Acta* **51,** 5746 (2006).
Janssen, G. J. M., *J. Power. Sources* **136,** 45 (2004).
Jao, T. J., Ke, S. T., Chi, P. H., Jung, G. B. and Chan, S. H., *Int. J. Hydrogen Energy* **35,** 6941 (2010).
Jeon, M. K., Won, J. Y., Oh, K. S., Lee, K. R. and Woo, S. I., *Electrochim. Acta* **53,** 447 (2007).
Jing, F. N., Hou, M., Shui, W. Y., Fu, J., Yu, H. M., Ming, P. W. and Yi, B. L., *J. Power. Sources* **166,** 172 (2007).
Kang, J. T. and Kim, J. B., *Int. J. Hydrogen Energy* **35,** 13125 (2010).
Kelly, M. J., Fafilek, G., Besenhard, J. O., Kronberger, H. and Nauer, G. E., *J. Power. Sources* **145,** 249 (2005).
Kim, J. T., Lee, J. H. and Tak, Y. S., *J. Power. Sources* **192,** 674 (2009).
Knights, S. D., Colbow, K. M., St. Pierre, J. and Wilkinson, D. P., *J. Power. Sources* **127,** 127 (2004).
Kundu, S., Simon, L. C. and Fowler, M. W., *Polym. Degrad. Stabil.* **93,** 214 (2008).
LaConti, A. B., Hamdan, M., McDonald, R. C. in W. Vielstich, A., Lamm, H. A., Gasteiger, (Eds), Handbook of Fuel Cells, vol. 3, John Wiley and Sons Ltd (2003), pp. 647–662.
Lamibrac, A., Maranzana, G., Lottin, O., Dillet, J., Mainka, J., Didierjean, S., Thomas, A. and Moyne, C., *J. Power. Sources* **196,** 9451 (2011).
Li, H., Song, C. H., Zhang, J. L. and Zhang, J. J., *In* ''PEM Fuel Cell Electrocatalysts and Catalyst Layers'' (J. J. Zhang, Ed.), Springer, London (2008).
Li, B., Lin, R., Yang, D. J. and Ma, J. X., *Int. J. Hydrogen Energy* **35,** 2814 (2010).
Liu, W., Ruth, K. and Rusch, G., *J. N. Mater. Electrochem. Syst.* **4,** 227 (2001).
Mani, P., Srivastava, R. and Strasser, P., *J. Power. Sources* **196,** 666 (2011).
Maranzana, G., Moyne, C., Dillet, J., Didierjean, S. and Lottin, O., *J. Power. Sources* **195,** 5990 (2010).
Mathias, M. F., Makharia, R., Gasteiger, H. A., Conley, J. J., Fuller, T. J., Gittleman, C. J., Kocha, S. F., Miller, D. P., Mittlesteadt, C. K., Xie, T., Yan, S. G. and Yu, P. T., *J. Electrochem. Soc. Interface* **14,** 24 (2005).
Meyers, J. P. and Darling, R. M., *J. Electrochem. Soc.* **153,** A1432 (2006).
Mohtadi, R., Lee, W. K. and van Zee, J. W., *J. Power. Sources* **138,** 216 (2004).
More, K. L., Microstructural characterization of PEM fuel cell MEAs. DOE H2 Program Review, May 2005, (2005).
Murthy, M., Esayian, M., Lee, W. K. and van Zee, J. W., *J. Electrochem. Soc.* **150,** A29 (2003).
Nagahara, Y., Sugawara, S. and Shinhara, K., *J. Power. Sources* **182,** 422 (2008).
Ohma, A., Yamamoto, S. and Shinohara, K., *J. Power. Sources* **182,** 39 (2008).
Okada, T., Ayato, Y., Yuasa, M. and Sekine, I., *J. Phys. Chem. B* **103,** 3315 (1999).
Okada, T., Ayato, Y., Satou, H., Yuasa, M. and Sekine, I., *J. Phys. Chem. B* **105,** 6980 (2001).

Oszcipok, M., Riemann, D., Kronenwett, U., Kreideweis, M. and Zedda, M., *J. Power. Sources* **145,** 407 (2005).
Panha, K., Fowler, M., Yuan, X. Z. and Wang, H. J., *Appl. Energy* **93,** 90–97 (2012).
Payne, T., ''Fuel Cells Durability and Performance''. The Knowledge Press Inc., US Brookline (2009).
Pereira, L. G. S., Paganin, V. A. and Ticianelli, E. A., *Electrochim. Acta* **54,** 1992 (2009).
Péron, J., Nédellec, Y., Jones, D. J. and Roziere, J., *J. Power. Sources* **185,** 1209 (2008).
Pourbaix, M., ''Atlas of Electrochemical Equilibria''. Pergamon Press, New York (1966).
Pozio, A., De Franceco, M., Cemmi, A., Cardellini, F. and Giorgi, L., *J. Power. Sources* **105,** 13 (2002).
Prabhuram, J., Krishnan, N. N., Choi, B., Lim, T. H., Ha, H. Y. and Kim, S. K., *Int. J. Hydrogen Energy* **35,** 6924 (2010).
Reiser, C. A., Bregoli, L., Patterson, T. W., Yi, J. S., Yang, J. D., Perry, M. L. and Jarvi, T. D., *Electrochem. Solid-State Lett.* **8,** A273 (2005).
Roen, L. M., Paik, C. H. and Jarvi, T. D., *Electrochem. Solid-State Lett.* **7,** A19 (2004).
Schlapka, A., Lischka, M., Groß, A., Käsberger, U. and Jakob, P., *Phys. Rev. Lett.* **91,** 016101 (2003).
Schmittinger, W. and Vahidi, A., *J. Power. Sources* **180,** 1 (2008).
Seo, D. H., Lee, J. H., Park, S. S., Rhee, J. K., Choi, S. W. and Shul, Y. G., *Int. J. Hydrogen Energy* **36,** 1828 (2011).
Shao, Y. Y., Yin, G. P., Gao, Y. Z. and Shi, P. F., *J. Electrochem. Soc.* **153,** A1093 (2006).
Shi, W. Y., Yi, B. L., Hou, M., Jing, F. N., Yu, H. M. and Ming, P. W., *J. Power. Sources* **164,** 272 (2007).
Siroma, Z., Kakitsubo, R., Fujiwara, N., Ioroi, T., Yamazaki, S. I. and Yasuda, K., *J. Power. Sources* **156,** 284 (2006).
Siu, A., Schmeisser, J. and Holdcroft, S., *J. Phys. Chem. B* **110,** 6072 (2006).
Soto, H. J., Lee, W. K., van Zee, J. W. and Murthy, M., *Electrochem. Solid-State Lett.* **6,** A133 (2003).
St. Pierre, J. and Jia, N., *J. N. Mater. Electrochem. Syst.* **5,** 263 (2002).
Takahashi, M., Kusunose, N., Aoki, M. and Seya, A., ''Abstract form Fuel Cell Seminar 2002''. Palm Springs, California (2002), 74.
Tang, H., Qi, Z. G., Ramani, M. and Elter, J. F., *J. Power. Sources* **158,** 1306 (2006).
Uribe, F. A. and Zawodzinski, T. A., *Electrochem. Acta* **47,** 3799 (2002).
Uribe, F. A., Gottesfeld, S. and Zawodzinski, T. A., *J. Electrochem. Soc.* **149,** A293 (2002).
Wagner, N. and Schulze, M., *Electrochim. Acta* **33,** 3899 (2003).
Wang, F., Tang, H. L., Pan, M. and Li, D. X., *Int. J. Hydrogen Energy* **33,** 2283–2288 (2008a).
Wang, Z. B., Zuo, P. J., Wang, X. P., Lou, J., Yang, B. Q. and Yin, G. P., *J. Power. Sources* **184,** 245 (2008b).
Wang, Y., Chen, K. S., Mishler, J., Cho, S. C. and Cordobes Adroher, X., *Appl. Energy* **88,** 981 (2011).
Washington, K., *in* Fuel Cell Seminar Abstract, Portland, p. 468. (2000).
Wasterlain, S., Candusso, D., Hissel, D., Harel, F., Bergman, P., Ménard, P. and Anwar, M., *J. Power. Sources* **195,** 984 (2010).
Wu, J. F., Yuan, X. Z., Martin, J. J., Wang, H., Zhang, J. Shen, J., et al., *J. Power. Sources* **184,** 104 (2008).
Wu, J. F., Yuan, X. Z., Martin, J. J., Wang, H. J. and Yang, D. J., *J. Power. Sources* **195,** 1171 (2010).
Xie, T. and Hayden, C. A., *Polymer* **48,** 5497 (2007).
Yang, D., Ma, J. X., Xu, L., Wu, M. Z. and Wang, H. J., *Electrochim. Acta* **51,** 4039 (2006).
Yoshida, H. and Miura, Y., *J. Membr. Sci.* **68,** 1 (1992).

Yousfi-Steiner, N., Mocoteguy, Ph., Candusso, D. and Hissel, D., *J. Power. Sources* **194,** 130 (2009).
Yu, X. and Ye, S., *J. Power. Sources* **172,** 145 (2007).
Yuan, X. Z., Li, H., Yang, S. S., Martin, J. and Wang, H. J., *J. Power. Sources* **196,** 9107 (2011).
Zamel, N. and Li, X. G., *Prog. Energy Comb. Sci.* **37,** 292–329 (2011).
Zhang, J. L., Tang, Y. H., Song, C. J., Xia, Z. T., Li, H., Wang, H. J. and Zhang, J., *J. Electrochim. Acta* **53,** 5135 (2008).
Zhang, S., Yuan, X. Z., Wang, H. J., Merida, W., Zhu, H., Shen, J., Wu, S. H. and Zhang, J. J., *Int. J. Hydrogen Energy* **34,** 388 (2009a).
Zhang, S., Yuan, X. Z., Hin, J. N. C., Wang, H., Friedrich, K. A. and Schulze, M., *J. Power. Sources* **194**(588), 588–600 (2009b).